https://doi.org/10.5194/egusphere-2025-2659
Preprint. Discussion started: 27 June 2025

Implications of Sea Breeze Circulations on Boundary Layer Aerosols in the Southern Coastal Texas Region

Tamanna Subba[1], Michael P. Jensen[1], Min Deng[1], Scott E. Giangrande[1], Mark C. Harvey[2], Ashish Singh[1], Die Wang[1], Maria Zawadowicz[1], Chongai Kuang[1]

[1]Environmental Science and Technologies, Brookhaven National Laboratory, Upton, NY, United States

[2]Department of Physics, Texas Southern University, Houston, TX, United States

Correspondence: Tamanna Subba (tsubba@bnl.gov)

Abstract

The Sea Breeze Circulation (SBC) influences atmospheric processes at multiple scales in coastal regions. Understanding how SBCs impact the aerosol number budget and aerosol impact on perturbation of incoming solar radiation is essential. This study investigates sea breeze–aerosol interactions (SAIs) during 46 summertime SBC events using data from the TRacking Aerosol Convection Interactions Experiment (TRACER) field campaign across rural and urban sites in southern Texas. Weather Research and Forecasting model coupled with Chemistry (WRF-Chem) simulations complement observations to explore spatio-temporal meteorological controls on boundary layer aerosols. During the campaign, Sea Breeze Fronts (SBF) penetrating inland transported cool, moist air over the land, introducing air masses with distinct properties compared to the preexisting continental air. These SAIs cause variability in number concentrations of up to a factor of two, with events typically lasting ~5 hrs before returning to background conditions. SAI's impact on aerosols varies with site's proximity to the sea and the preceding sea breeze (SB) history, primarily affecting the marine-influenced accumulation mode. The coastal site reflects stronger marine influence, while the inland site reflects SB air masses that regain continental characteristics. Model outputs show that the regional SAIs extend ~50 km inland and reach up to the boundary layer height. SBC further influences the local aerosol radiative impacts by changing the aerosol number budget. SAIs modify cloud condensation nuclei in ~20% of events during SBF passage. For the typical TRACER SBF passage, the local aerosol radiative forcing was also found to change by up to 40%.

https://doi.org/10.5194/egusphere-2025-2659
Preprint. Discussion started: 27 June 2025

1 Introduction

A significant portion of the global population resides in coastal cities, including several megacities (Brown et al., 2013). Nearly half of the U.S. population faces environmental challenges associated with complexities tied to urban coastal atmospheres (Crossett et al., 2004; Hudson et al., 2012). Houston, located along the Southern Texas coastline, is one of the United States' most populated cities, while also one of its most polluted, with high aerosol concentrations (Yoon et. al., 1994; Kleinman et al., 2002; Banta et al., 2011). These aerosol particles can have regional adverse effects on human health (Partanen et al 2018; Mack et al., 2020), while on the global scales impacting Earth's energy balance. These impacts may be felt directly through aerosol scattering and absorbing the incoming solar radiation (Charlson et al., 1992; Bond et al., 2013; IPCC, 2021), and/or indirectly through aerosol influence on clouds and precipitation as cloud condensation nuclei (CCN) and ice nucleating particles (INP) (Twomey, 1974; Albrecht et al., 1989; Ramanathan et al., 2001; Rosenfeld et al., 2008; Ariya et al., 2009; Burkart et al., 2021). In particular, the Houston region experiences highly complex aerosol processes due to elevated local emissions, diverse aerosol sources, and intricate atmospheric chemistry. Understanding complex aerosol processes around Houston is further complicated as the regional meteorology may be influenced by sea breeze circulations (SBC, e.g., Miller et al., 2003; Wang et al., 2024; Deng et al., 2025). The SBC is a mesoscale meteorological phenomenon that develops regularly along coastal regions (Miller et al., 2003). One key challenge for aerosol process studies common to coastal city environments is in determining the relative importance of aerosol microphysical versus mesoscale meteorological controls such as SBCs in governing the aerosol number budget and aerosol impacts on that population center.

The summertime SBC is a thermally-driven feature tied to differential heating between the land and sea; this results in density gradients that cause the cooler marine air to propagate inland (Miller et al., 2003; di Bernardino et al., 2021). Daytime SBC formation can facilitate convective cloud and precipitation onset (Comin et al., 2015), influence boundary layer meteorology (Adaricheva et al., 2023), and has been associated with complex impacts on overall air quality (Simpson, 1994; Masselink and Pattiaratchi, 1998; Moorthy et al., 2003; Miller et al., 2003; Augustin, et al., 2020; Park et al., 2020; Parajuli et al., 2022; Wang et al., 2023). These circulations also influence transport of atmospheric gases (Gangoiti et al., 2001;

https://doi.org/10.5194/egusphere-2025-2659
Preprint. Discussion started: 27 June 2025

Ahmadov et al., 2007; Hernández-Ceballos et al., 2015) and aerosol particles (Clappier et al., 1999; Borge et al., 2008; Papanastasiou et al., 2010). A sea breeze front (SBF), which is the boundary between that cooler, stable marine air of the SBC flow and the warmer, unstable air over the land, is often a focal point that facilitates the transport and dispersal of aerosols, as well as aiding in the formation of cumulus clouds (Miller et al., 2003). Moreover, locations along the SBF often exhibit an enhancement in upward air motion, allowing aerosols to ascend to higher altitudes ~2 km (Iwai et al., 2011). Stronger wind shear along these SBFs also generates increased turbulence, as owing to Kelvin-Helmholtz instability occurring just behind this front (Linden and Simpson, 1986; Plant and Keith, 2007), while the aforementioned vertical air motions are important for convective cloud initiation (Rao and Fuelberg, 2000; Arrillaga et al., 2020).

The common conceptual model for SBCs is one where the marine air mass propagates inland, bringing with it different atmospheric and aerosol characteristics compared to the ambient land air mass conditions. In this study, we term any influence these SBCs have on regional aerosols as “sea breeze - aerosol interaction” (SAI). Previous studies have shown that SAIs vary depending on complex interactions among emissions sources, boundary layer dynamics, and the strength and/or direction of SBC. For example, SBF passage has been previously found to trap aerosols at lower elevations within the boundary layer (Miller et al., 2003). The competition between converging winds associated with the front, and the vertical air mixing over the land, controls this lifting of aerosols (Simpson, 1994; di Bernardino et al., 2021). As a result, aerosols may be confined within the shallow thermal boundary layer (i.e., the lowest layer in direct contact with the surface), leading to increased surface aerosol concentrations (Boyouk et al., 2011; di Bernardino et al., 2021). On the other hand, SBCs may also replace the regional air mass with the cleaner marine air mass, leading to a decrease in surface aerosol concentration. This now-modified coastal environment can affect the generation and growth of aerosols, impacting the local aerosol number budget that further influences their direct and indirect effects.

Although several studies have investigated the overall change in the aerosol loading during SBC events, less is known about the role of SAI on the aerosol microphysical properties. Moorthy et al. (1993) observed that the passage of the SBF was associated with increase in the concentration of the smaller particles during passage of the SBF. Furthermore, since SBFs propagate inland, SBCs can have far-reaching impacts on aerosol properties (Iwai et al., 2011;

https://doi.org/10.5194/egusphere-2025-2659
Preprint. Discussion started: 27 June 2025

Park and van den Heever, 2022). As an example, previous studies conducted in the Southeastern United States indicated that inland propagating SBFs are followed by air masses that often contrast with regional air, oriented parallel and traveling perpendicular to the coastline to distances 220 km from the Gulf of Mexico (Viner et al., 2021; Bao et al., 2023). Inland SBF propagation may also bring additional aerosol property implications throughout and above the boundary layer. Parajuli et al. (2020) found that the SBC influences the aerosol vertical distribution over the eastern coast of the Red Sea while lifting dust aerosols along the western slope of the Sarawat mountains. Similarly, enhanced turbulent activity along the SBF was associated with vertical aerosol transport above the boundary layer top (~1.1 km a.s.l) for a flat coastal area of the North Sea (Talbot et al., 2007).

As introduced above, the Houston-Galveston-Brazoria region in Texas is the fourth-largest metropolitan area in the United States with a population exceeding 6 million people (Li et al., 2020). High aerosol concentrations in the Houston area are linked to strong surface emissions and meteorological conditions (Wert et al., 2003; Ryerson et al., 2003). This metro region is also home to numerous petrochemical factories that are one of the sources of anthropogenic emissions. Several studies have also shown that meteorological conditions around Houston are highly susceptible to the interaction between large-scale (background) geostrophic flows and mesoscale SBCs (Miller, 2003; Wang et al., 2024; Deng et al., 2025). Our motivation is to investigate the role of SAIs as observed over a complex urban megacity region, and specifically document SBC influence on aerosol microphysical properties. These efforts expand on previous Houston studies such as Li et al. (2020) who employed a K-Means clustering algorithm to study the relationship between Houston-region SBCs and the daily ozone variability during the DISCOVER-AQ (Deriving Information on Surface Conditions from Column and Vertically Resolved Observations Relevant to Air Quality) field campaign.

This study capitalizes on the recent TRacking Aerosol Convection Interactions ExpeRiment (TRACER) field campaign conducted by the US Department of Energy (DOE) Atmospheric Radiation Measurement (ARM) user facility (Mather and Voyles, 2013), which took place from October 1, 2021, to September 30, 2022 (Jensen et al., 2022). The main TRACER field site was placed at an urban coastal location in Houston, and additional observations were made at a rural site in southern Texas during an intensive observation period (IOP) from June 1 to September 30, 2022. Using these TRACER-IOP measurements, our study will explore how these SBCs influence the aerosol environment at multiple ground sites. In

https://doi.org/10.5194/egusphere-2025-2659
Preprint. Discussion started: 27 June 2025

addition, we will use targeted Weather Research and Forecasting modeling coupled with Chemistry (WRF-Chem) to investigate the regional impacts of SAI over Southern Texas. A detailed description of the TRACER sites, instruments, measurements, and methodology, followed by the WRF-Chem model configuration details, are presented in Section 2. Section 3 presents our campaign observational and simulated results. Our efforts will characterize the composite meteorological (Section 3.1) and aerosol (Section 3.2) observations during the IOP at the primary TRACER urban and rural sites. This is followed by a composite analysis of the observed effects of the sea breeze on aerosol properties at the two ARM sites (Section 3.3), as well as a detailed case study examination of SAI influence for these locations (Section 3.4). The regional influence of SAI is further explored using model simulations, as demonstrated for the horizontal (Section 3.5) and vertical propagation of SAIs (Section 3.6), and SAI impact on cloud condensation nuclei and local aerosol radiative forcing over the southern Texas region (Section 3.7). The study concludes with our key findings summarized in Section 4.

2 Data and methods

2.1 Site description

The DOE ARM's TRACER field campaign was centered on the deployment of the first ARM Mobile Facility (Miller et al., 2016, AMF1) and its main instrument site (M1) (Fig. 1). The M1 is an urban coastal site located at the La Porte, Texas (TX) airport, to the south of Houston, TX. Given the high propensity for isolated convective cloud events during summertime months (Jensen et al., 2022), the TRACER IOP was conducted from June 1 to September 30, 2022, with a goal towards sampling a range of aerosol-cloud interactions during these convective events. Additional ARM and guest instruments were deployed to an ancillary site (S3) during this TRACER IOP as also documented in Jensen et al. (2022). This S3 supplemental site is a rural site in Guy, TX, located ~70 km west from M1, upstream and periphery to the highly populated and commercial sectors of the Houston-Galveston-Brazoria region. The southern Texas region is characterized by flat terrain with elevations < 50 m a.s.l and a diversity of land cover/use, including urban, rural, grassland, and forested coastal environments (see Fig. 2a). As in TRACER's overarching motivations, the Houston region is frequented by isolated convective clouds that interact with ambient aerosol conditions from the urban and industrial sources, potentially serving as a natural contrast to clouds that form in

https://doi.org/10.5194/egusphere-2025-2659
Preprint. Discussion started: 27 June 2025

surrounding areas that exhibit significantly lower background aerosol concentrations (Banta et al., 2005; Parrish et al., 2009; Wang et al., 2024).

2.2 Measurements of aerosols and meteorological properties

This study focuses on the enhanced aerosol and complementary observations available during the TRACER summertime IOP period. The key aerosol datasets available during this IOP include: (1) the aerosol number size distribution and total number concentration, (2) bulk aerosol chemical composition, and (3) state meteorological properties (e.g., surface temperature, humidity). Campaign availability of in-situ observations at two contrasting sites provided an excellent opportunity to understand the regional aspects of SAI.

The aerosol number size distribution with diameter ranging from 10 to 500 nm was measured at M1 and S3 sites using Scanning Mobility Particle Sizer (SMPS) (Singh and Kuang, 2024). The aerosol number size distributions (dN/dlogDp) at different diameters (Dp) were added to calculate the total integrated aerosol number concentrations. Bulk aerosol chemical compositions consisting of total organics, sulfate, nitrate, ammonium, and chloride were measured at M1 and S3 sites using Aerosol Chemical Speciation Monitor (ACSM) (Watson, 2017). Surface meteorological variables: temperature, relative humidity (RH), rainfall, wind direction and wind speed at M1 and S3 sites were taken from the meteorological instruments collocated with the aerosol instruments. These instruments are part of the operating Aerosol Observing Systems (AOS), which is the primary platform for in situ aerosol measurements at Earth's surface (Uin et al., 2019). All data were averaged to 5-minute intervals.

To supplement those observations, we used the measured particulate matter of 2.5 micrometers or less in diameter ($PM_{2.5}$) mass concentrations from the Texas Commission on Environmental Quality (TCEQ) database (Shrestha et al., 2023). The TCEQ operates a network of surface air quality monitoring stations throughout Texas, with network observations capturing several key air quality indicators, including ozone, $PM_{2.5}$, sulfur dioxide, and benzene. The TCEQ site at Seabrook Friendship Park (C45, 29.583°N, -95.016°E), the location nearest to the M1 site, was used in the analysis.

2.3 Model simulation setup

https://doi.org/10.5194/egusphere-2025-2659
Preprint. Discussion started: 27 June 2025

We use the WRF-Chem model (Grell et al. 2005; Skamarock et al., 2008) to simulate the multiscale interactions between aerosols and meteorology over the coastal region of Houston. In Fig. 2, we show the implemented model domain that was centered on the M1 site and extended from 26 to 33 ºN (~770 km) in latitude and from -98.5 to -91.5 ºE (~670 km) in longitude. The model simulations were conducted from 01 July 2022 to 30 August 2022, using a 5x5 km horizontal grid spacing with 45 vertical layers. Simulations used meteorological boundary conditions from North America mesoscale (NAM), and anthropogenic emission inventory from National Emissions Inventory (NEI) (Ma and Tong, 2022), and biogenic emissions from the Model of Emissions of Gases and Aerosols from Nature version MEGAN v2.1 (Guenther et al., 2012). The model simulations were performed with full aerosol-gas chemistry, and land-atmosphere interactions enabled. The geogrid component of the WRF Processing System handles the land use data (Fig. 2a). The grid spacing and configuration is assumed sufficient to capture the salient meteorology suitable to the aerosol chemistry considered. The details of the configurations are shown in Table 1.

The area surrounding the M1 site is primarily characterized by urban infrastructure and cropland, whereas the S3 site is largely a mix of cropland, natural mosaic, and barren or sparsely vegetated land type. Both sites are positioned with cropland and grassland in directions west and north, as well as evergreen, deciduous, and mixed forests conditions to north to east directions. The selected domain included both anthropogenic and biogenic aerosol sources, as indicated by NEI and MEGAN datasets (Fig. 2b). The M1 site is anticipated to be more influenced by anthropogenic sources due to its proximity to the Houston urban core, local industry and the shipping channel. The S3 site is expected to be more influenced by biogenic sources.

The role for these simulations is to provide a physically-reasonable approximation for the meteorological and aerosol environments across the southern Texas region that are not captured by the point measurements during TRACER. When compared with the TRACER measurements, the simulated meteorological time series show feasible agreement at both sites (Fig. S1). We also compare the simulated hourly $PM_{2.5}$ with the TCEQ measured values (Fig. 3a). The model reasonably captures the timings and magnitude of high and low aerosol concentrations. Our model (mean ~ 10.8 μg m^{-3}, median ~8.5 μg m^{-3}) does overestimate these concentration measurements (mean ~8.2 μg m^{-3}, median ~7.0 μg m^{-3}), with r ~0.6 (difference in mean ~30%; difference in median ~ 23%). We see a reasonable behavior in heterogeneous

https://doi.org/10.5194/egusphere-2025-2659
Preprint. Discussion started: 27 June 2025

spatial distribution of $PM_{2.5}$, with higher values in the urban areas around the M1 site and lower values in the rural areas around the S3 site (Fig. 3b). Previous studies have reported similar discrepancies between measured and modeled aerosol concentrations. For example, Soni et al. (2022) found that WRF-Chem simulations during dust storm events over the Indian sub-continent reasonably captured the spatial aerosol patterns, however underestimated concentrations in areas with high aerosol loading. Tuccella et al. (2012) similarly found that the WRF-Chem model captured the variability induced by high aerosol concentration periods but underestimated the magnitude of these periods by 7.3%. Recently, Georgiou et al. (2022) also reported that WRF-Chem underestimates background $PM_{2.5}$ concentrations by about 16%, and by 20% at industrial stations.

3 Results and discussion

3.1 Composite IOP Meteorological Observations

The M1 site was uniquely situated for TRACER campaign aerosol-cloud studies owing to its proximity to the Galveston Bay coastline (1.5 km) and the Gulf of Mexico (~55 km). The S3 site was located farther from the Galveston Bay however nearer to the Gulf of Mexico, thus expected to experience varying rural to urban influences on its meteorological and aerosol conditions. During the IOP, the measured daily average temperatures at these locations ranged from 24 to 31 °C. Wind speeds are higher at the M1 site, ranging from 1.5 to 5.3 m s^{-1} as compared to 0.9 to 3.6 m s^{-1} at the S3 site. The RH at both the locations showed daily averaged values of ~75%. At both M1 and S3 sites, the winds generally arrive from the northeast to the southwest.

Fig. 4. shows the diurnal variation of meteorological properties averaged during the IOP. While comparing meteorological variables between M1 and S3 sites, paired t-test results show a very low p-value (<0.0001) and a large negative or positive t-statistic, indicating a statistically significant difference between the two sites. Compared to S3, M1 exhibits higher temperatures during the cooler parts of the day (early morning) and slightly lower temperatures during the warmest parts of the day (early afternoon). The opposite trend is observed for RH, with M1 showing lower RH values during the cooler periods and higher values during the warmer periods of the day. These values are comparable during the morning (~14:00–15:00 UTC) and

https://doi.org/10.5194/egusphere-2025-2659
Preprint. Discussion started: 27 June 2025

late evening (~23:00–00:00 UTC) hours. Wind speeds are approximately 1 m s^{-1} higher at M1 throughout the day, except during the morning hours. On the other hand, wind directions are comparable throughout the day, except during the late night to morning hours, when the average direction changes by about 45 degrees. Although the M1 and S3 sites are located near each other, their different proximities to water bodies and varying land cover types may account for the meteorological variations between the two. In addition to the geographic positioning, S3 being a rural site, has land surface covered with predominant vegetation and soil, which cool faster at night (lower T and higher RH). During the day, they heat up quickly (higher T and lower RH). The opposite happens over the urban site with surfaces covered with concrete and asphalt, which retain heat, staying warmer at night, and moderating temperatures during the day.

Wang et al. (2024) studied synoptic-scale controls affecting SBC evolution and cloud formation at the two sites. A total of 46 SBC events at the M1 site, and 31 SB events at the S3 site were identified during the IOP using a combination of satellite and ground-based measurements. Most of these cases are under the control of anticyclonic systems (Wang et al., 2022). The SBF timing at both ARM sites is identified using surface wind and water vapor mixing ratio time series. They found that the SBF typically arrived at the M1 site at around 20:30 UTC (i.e., 15:30 LT), and at the S3 site at around 20:50 UTC (i.e., 15:50 LT). In this study, we use all the SBC days identified by Wang et al. (2024) to understand the SAI during IOP.

3.2 Composite IOP Aerosol Observations

The southern Texas region is influenced by locally-generated (e.g., vehicular, industrial, construction and road dust, and sea spray) and long range transported aerosols (e.g., biomass burning, mineral dust, and sea spray) from anthropogenic and natural sources (Brown et al., 2002; Barrett and Sheesley, 2014; Karnae and John, 2019; Song et al., 2021; Das et al., 2023; Shrestha et al., 2023). The measured aerosol number concentration during the IOP shows a significant day-to-day variability ranging from 0.2 e^4 to 2.0 e^4 particles cm^{-3}. In Fig. 5a, we plot the diurnal distribution of aerosol number concentration, with these values peaking at around 17:00 UTC at the M1 site, and at around 20:00 UTC at the S3 site (Fig. 5a.). Both sites exhibit a tri-modal aerosol size distribution (Fig. 5b.). Throughout the day, the aerosol

https://doi.org/10.5194/egusphere-2025-2659
Preprint. Discussion started: 27 June 2025

concentrations are consistently higher at the M1 site when compared to those observed at the S3 site. At the M1 site, we observe a distinct nucleation mode that appears at diameter <20 nm, and two additional modes at larger diameters ~80 nm and ~150 nm. This nucleation mode is less prominent at the S3 site, which more commonly exhibits similar modes at diameters ~80 nm and ~150 nm.

The aerosol bulk mass concentration ranged from 1.6 μg m^{-3} at the IOP start in June to 6.3 μg m^{-3} by September at the M1 site. These values did not differ from those collected within the marine coastal environment of our ancillary S3 site, ranging from 1.4 μg m^{-3} in July to 7.1 μg m^{-3} in September. The ACSM suggested a similar percentage contribution from various species, with organics having the highest concentration (45% at M1 and 55% at S3), followed by sulfate (36% at M1 and 32% at S3), ammonium (15% at M1 and 7% at S3), and chloride (less than 4% at M1, and less than 5% at S3). Higher percentages of organics and sulfate are consistent with the measurements at both urban (Minguillón et al., 2015; Huang et al., 2010; Qi et al., 2020) and rural locations (Crippa et al., 2014; Atabakhsh et al., 2023). On average, organics and ammonium are approximately 1.5 and 3.0 times higher at M1, respectively, while sulfate is slightly higher at S3 by about 1.2 times.

New particle formation (NPF), a microphysical process by which new particles are formed directly from the gas phase precursors, significantly affects the aerosol number budget in the atmosphere (Kulmala et al., 2004, 2014; Kuang et al., 2009, 2012; Kerminen et al., 2018). NPF events were common at M1 and S3 sites. During summertime, M1 (22 events) and S3 (18 events) identified a comparable number of NPF events. The majority of these NPF events exhibited a clear nucleation mode followed by a steady growth. On approximately 35% of NPF events, we observed regional NPF events occurring simultaneously at both the M1 and S3 sites. These regional NPF nucleation modes appear at Dp < 25 nm and grow consistently across a broader region, covering a minimum radius of tens of kilometers. However, these co-occurring NPF events displayed different characteristics in terms of their duration and growth, hinting at the possible influence of mesoscale to larger-scale meteorological controls on these processes, the background, aerosol, and the availability of necessary precursors. One of those potential meteorological controls that may influence these events is SAI, to be explored in the later sections.

https://doi.org/10.5194/egusphere-2025-2659
Preprint. Discussion started: 27 June 2025

3.3 Observed Sea Breeze aerosol interaction at the surface

Wang et al. (2024) showed that both M1 and S3 sites fall within the region influenced by SBC. Coastal regions have a mixture of urban, terrestrial, and marine aerosol regimes. The inland-penetrating SBF can have a complex influence on the aerosols over this location depending on several coexisting factors including: (i) pre-existing aerosol regime over the location, (ii) the aerosol regime of the new air mass preceded by the SBF, (iii) the local and synoptic thermodynamic conditions resulting to convective boundary layer features such as formation of horizontal convective rolls, and (iv) the characteristics of the SBF itself (for example, the lifting and mixing of the onshore flow with the ambient air, wind anomalies near the surface, and the extent of the SB lifecycle). For any inland-penetrating SBF, the authors find it instructive to define three possible scenarios for the influence of any inland-penetrating SBF on aerosols within the region of influence. First there is a potential "reduction influence", which occurs when an air mass with higher aerosol concentration over a location is replaced by an air mass with lower aerosol concentration. Next, there may be an "enhancement influence", which occurs when an air mass with lower aerosol concentration over a location is replaced by an air mass with higher aerosol concentration. Finally, a "neutral influence" implies minimal change, defined as a change in the aerosol concentration is less than 5% in the pre-existing aerosol regime, indicating that the new air mass introduced by the SBF is similar to the existing conditions. For example, an enhancement influence may occur when long-range transported aerosols are present in the air mass downwind of this SBF, or when the SBF first advects over areas (marine or continental) with high local emissions. Similarly, we anticipate neutral influences when the entire region has relatively homogeneous (i.e., similar aerosol concentrations also belonging to the same aerosol regime) distribution of aerosols. However, aerosol exchanges are complex, as demonstrated by the examples from the TRACER campaign, where marine aerosols carried by the SBF also exhibited negligible influences on the ambient marine aerosol mode.

As one approach to investigate the influence of SAI on the surface aerosol concentration, we normalized the aerosol concentration at time (T) with the concentration of aerosols measured just before the passing of the SBF (T_{SBF}=0 hr). Here, "just before" refers to the five minutes prior to the SBF passage, as previously identified by Wang et al. (2024) (refer to section 3.1). In Figs. S2 and S3, we provide the temporal variation of this normalized aerosol

https://doi.org/10.5194/egusphere-2025-2659
Preprint. Discussion started: 27 June 2025

number concentration for all the SB events. At the continental sites, before-SBF aerosol concentrations can vary by up to a factor of two.

Example days with an "enhancement influence" in the aerosol concentration after T_{SBF} are shown in Fig. 6a, highlighting the 18 July event at the M1 site, and a 10 August event at the S3 site. In contrast, the 17 June (M1 site) and 10 July (S3 site) events in the same figure help illustrate a "reduction influence" in aerosol concentration after T_{SBF}. While these example events are instructive, there is not a clean conceptual model for TRACER events given the high level of variability in the duration or influence of SAIs. For example, the sharp increase we observe in aerosol concentration on the 10 August "enhancement" event quickly disappears within an hour after T_{SBF} at the S3 site. In contrast, the increase in the number concentration we observed on 18 July persisted for over an hour after T_{SBF}. Considering all the SBF passages we collected, we suggest $\Delta T = T_{SBF} \pm 1$ hr often best represents the "before" ($\Delta T_- = T_{SBF} - 1$ hr) and "after"- SBF ($\Delta T_+ = T_{SBF} + 1$ hr) times over a location. With that assumption, a percentage change of the aerosol number concentration [(after-before)/before x 100%] can be further calculated. 'Neutral influence' days with the change in aerosol concentration <5% are not considered in this analysis.

The M1 site (60% of the SB days) experiences more frequent changes in surface aerosol concentrations due to SAI compared to S3 (34% of the SB days). On average, the aerosol number concentration decreases by ~25% (from 9.8x 10^3 cm^{-3} during ΔT_- to 7.2x 10^3 cm^{-3} during ΔT_+) at the M1 site. On the other hand, the aerosol number concentration increases by ~7% at the S3 site (from 3.8x 10^3 cm^{-3} during ΔT_- to 4.1x 10^3 cm^{-3} during ΔT_+). Total of 16 events at the M1 site and 4 events at the S3 site showed a reduction influence, whereas 13 and 8 SB days showed enhancement influence, and 9 and 13 SB days showed neutral influence on the measured aerosol concentrations, respectively. These discrepancies highlight the regional variability associated with SAI events. As previously mentioned, the geographical positioning of M1 and S3 sites could be one of the reasons for such variabilities. M1 is more influenced by the Bay breeze coming from Galveston Bay and S3 is more likely influenced by Gulf breeze from Gulf of Mexico. Even if the air mass associated with the SBF contains lower aerosol concentration, the longer distance the SBF travels to reach the S3 site allows the marine air mass to mix with the continental air mass, potentially resulting in higher aerosol concentrations, and vice versa.

https://doi.org/10.5194/egusphere-2025-2659
Preprint. Discussion started: 27 June 2025

We suggest that SAIs can potentially interfere with aerosol microphysical processes, including NPF. A total of 11 NPF events occurred during SB events. Out of those, ~5 days showed a distinct change in the NPF characteristics during the passing of the SBF. For example, an NPF event that occurred at the M1 site on 16 July during before-SBF hours (Fig. S4). Upon the arrival of the SBF during this event, particle growth abruptly ceased, and the elevated particle concentration (~14 e^3 particles cm^{-3}) observed during this NPF event simultaneously decreased to ~5 e^3 particles cm^{-3} (Fig. S4). During the days where there were ongoing NPF events, the aerosol concentrations were high during the before-SBF period ($\Delta T_{-}=T_{SBF}$ - 1 hr). The cleaner air mass trailing the SBF passage led to a sharp reduction in the aerosol number concentrations in the after-SBF period ($\Delta T_{+}=T_{SBF}$ + 1 hr).

The open-air polar plots summarize the relationship between aerosol number concentration, wind speed and wind direction within $\Delta T= T_{SBF}\pm1$ during all the SB events (Fig. 6b.). Our supplemental Fig. S5 also indicates that overall aerosol concentrations at the M1 site are higher when the prevailing winds emanate from the east and north directions associated with the Houston urban core (specially in August and September). Overall, the passage of SBF at M1 is marked by an increase in wind speed and a shift in dominant wind direction toward the southeast and intermediate directions. This transition is consistently accompanied by a reduction in aerosol number concentrations relative to the before-SBF aerosol concentrations, confirming that SBFs transport marine air with lower aerosol concentrations. However, concentrations are observed to be higher on days associated with a higher aerosol loaded marine air mass. The S3 site responds similarly to the M1 site, however the average change in aerosol concentration from before-SBF to after-SBF condition suggests only a small increase from ~3.9 e^3 to ~4.1 e^3 particles cm^{-3} (Figs. 6b., S3. and S5.).

These TRACER results are consistent with previous studies showing that northerly winds bring continental air with higher aerosol concentrations, while southerly winds bring clean marine air to southern Texas (Levy et al., 2013; Pinto et al., 2014). Wind direction reversals bring aged aerosol loaded plumes with high O_3 and NO_x levels back to the Houston area (Pinto et al., 2014). Occasional increases in aerosol concentrations at M1 and S3 sites can also be associated with long-range transported aerosols. Summertime conditions are notably influenced by episodic transboundary aerosol transport (Das et al., 2023), including dust events from the Sahara Desert (Aldhaif et al., 2020) and biomass burning events in Central America and its neighboring states. The biomass burning includes both the prescribed agricultural fires

https://doi.org/10.5194/egusphere-2025-2659
Preprint. Discussion started: 27 June 2025

in Central America (Wang et al., 2018) and forest fires in surrounding states (Westenbarger and Morris, 2018). Central America biomass burning contributes to half of the biomass burning PM concentrations in Houston (Das et al., 2023). The Bermuda-Azores High helps dust originates in the far west to transport to the southeast coast (Perry et al., 1997; Bozlaker et al., 2013). This synoptic system and the mesoscale atmospheric circulation combine to influence the aerosol transport (Mao et al., 2020).

3.4. Examples of sea breeze aerosol interaction at TRACER

In Fig. 7, we provide an example of an aerosol reduction influence of SAI. Since M1 and S3 both experienced SB on 10 July, this day serves as a good example to investigate how SAIs evolve when simultaneously viewed at multiple sites. The SBF reached the M1 site in the afternoon at around 21:30 UTC, and the S3 site at around 23:45 UTC. In Fig. S6, we supplement these discussions with displays for the temporal variation of measured and model-simulated meteorological properties for this event. Both sites suggest the typical temperature decreases and surface wind speed increase associated with the SBF reaching the site. The wind direction changes from east to south at the M1 site and from southwest to south at the S3 site.

The changes in aerosol size distribution, reduction in the bulk chemical composition, and simulated $PM_{2.5}$ all suggest that the air mass following SBF passage contains lower aerosol concentration (Fig. 7.). This likely indicates that during the after-SBF period, the air mass is arriving from directions less influenced by the aerosol sources. The changes in aerosol size distribution, reduction in bulk chemical composition, and simulated $PM_{2.5}$ all suggest that the air mass following the SBF passage contains lower aerosol concentrations. The SBF acts as a leading edge of this cleaner marine air mass. The aerosol number concentration decreases by ~5% (5.2 e^2 cm^{-3}) at the M1 site. At the M1 site, there was no significant change in the mean Dp (~100 nm) during the first 45 min after T_{SBF}, which is followed by a sharp decrease in the mean Dp (~25 nm). This change in the aerosol number concentration is synchronous with the changes in wind direction from east to south (polar plots in Fig. 7a), consistent with a more marine aerosol environment.

Immediately after the passing of the SBF at the S3 site, the SAI also suggests a reduced influence of ~62% (3.3 e^3 cm^{-3}) in terms of the aerosol number concentration, (Fig. 7b). However, the background aerosol mode persists at diameters ~60 and 150 nm (aerosol size

https://doi.org/10.5194/egusphere-2025-2659
Preprint. Discussion started: 27 June 2025

distribution plot in Fig. 7b). Note, we did not observe a profound change in the wind directions after the passing of the SBF at the S3 site. However, we suggest the higher wind speed associated with the SBF dilutes the existing air mass with that from the marine air mass with lower aerosol concentration. The modified near-surface air mass at S3 persists overnight until convective mixing begins the following day.

In Figs. S7 and S8, we provide additional examples from TRACER SAI events. The first example is from the 17 July event where we observed an increased influence in the aerosol concentration that followed SBF passage. The increased influence continued for the next ~2 hours. The second example is from 16 August that illustrates a neutral influence event on the aerosol concentrations following the passing of the SBF. Detailed discussions on these example events will be continued in the next section that expands this discussion to include regional removal and transport influences on these SAI events.

3.5. Regional influence of sea-breeze aerosol interaction

In Fig. 8, we provide the spatial distribution of modeled water vapor mixing ratio, planetary boundary layer height (PBLH), surface-level wind vectors, $PM_{2.5}$, and integrated aerosol number concentration (nucleation-nu0 + accumulation-ac0 mode) using WRF-Chem. On 10 July, the observed SBF reached the M1 site at 21:30 UTC and reached the S3 site at 23:40 UTC. The model simulation for this event accurately represents this timing for the SBF passage. The model output for the time 20:00 UTC on 10 July corresponds to an example point in the model runs and daytime observations when the SBF had not reached either site. The 22:00 UTC model examples correspond to a time when the modeled and observed SBF has recently passed the M1 site but not reached the S3 site. The 00:00 UTC examples (next day) correspond to a timing when the SBF has passed both TRACER field sites.

Behind the SBF in our simulations, south or southeast winds prevail, passing through from the Gulf of Mexico and blowing onshore at an average speed of 5 m s^{-1}. There is an increase in water vapor mixing ratio associated with the SBF passage. This transition in the air mass is also observed around the M1 site at timestep 22:00 UTC. A similar pattern in the water vapor mixing ratio is observed at the S3 site at the timestep 00:00 UTC. This change at S3 is also accompanied by a decrease in the modeled PBLH (Fig. 8).

https://doi.org/10.5194/egusphere-2025-2659
Preprint. Discussion started: 27 June 2025

The 10 July event simulations also help illustrate that while changes in aerosol and meteorological properties are more pronounced near the SBF, SBF influences may extend >50 km inland associated with the path and extent of this feature. Along the convergence zone associated with the SBF, particle concentrations are higher ahead of the SBF and lower behind it, due to intrusion of cleaner marine air into the convergence zone. Consequently, SBF passage in the model creates a swath of reduced aerosol concentration (up to 50%) parallel to the Galveston Bay or Gulf of Mexico coastline (Fig. 8). Over time, this lower concentration area moves towards northwest, with the SBF's influence diminishing as the air mass travels farther inland.

Fig. 9 provides additional examples from the remaining reference TRACER scenarios, the 17 July event suggestive of an enhancement in aerosol concentration associated with the SBF, and the 16 August case indicative of a neutral influence from the SBF passage. First, it is noteworthy that the simulation set-up for the 17 July event exhibits a very different ambient aerosol environment when compared to the previous 10 July event. The aerosol mass concentrations over the marine environment for this event are higher than those observed over land (Fig. 9a). The high concentrations are also observed to be more prominent to the southwest of the M1 site. Hence, as the SBF moves inland on 17 July, it transports this higher aerosol containing air mass, replacing the lower aerosol containing air over the site and causing an increased aerosol concentration at the M1 site (Fig. 9b). The onshore winds carry air mass influenced by both local and long-range transport, originating from both land and sea. In contrast to the other event simulations, the 16 August event features an aerosol environment that was notably uniform over the wider regional air masses, thus SBF passage resulted in minimal changes to the aerosol distribution (Fig. 9c, d).

From these simulated event examples, it is perhaps not surprising that the effect of the inland-penetrating SBF on the aerosol environment appears highly dependent on the pre-existing aerosol condition over the location, as well as the air mass characteristics trailing the SBF. For TRACER examples, the inland propagation of regional SBFs extends up to 50 km from the coastline, with wind speeds reaching up to ~7 m s^{-1}. These behaviors are consistent with available observations. Boundary layer wind field analysis using scanning radar data during TRACER supports our findings that there is reduced influence on the aerosol concentration immediately after the passing of the bay breeze front for the next few hours, due to the dominance of onshore flow (Deng et al., 2025). However, the wind anomaly associated

https://doi.org/10.5194/egusphere-2025-2659
Preprint. Discussion started: 27 June 2025

with the gulf breeze front can lead to increased aerosol concentration as it passes over the M1 site during the subsequent 5 hour period.

3.6 Sea breeze effects on vertical distribution of aerosols

Fig. 10a shows the modeled normalized $PM_{2.5}$ at different elevations before and after the passage of the SBF. On 10 July, the cleaner marine air mass that follows the SBF led to a decrease in aerosol concentration below 1 km at the ARM sites. The model also shows surface convergence along the SBF (Fig. S9.). The aerosol concentrations are redistributed horizontally and vertically. The model indicates that cleaner air mass shifts to a distance approximately 50 km inland from the M1 site. Two hours later, the SBF reaches the S3 site where its passage causes a similar change in the aerosol concentration. The varying extent of this air mass and its inland propagation redistributes the vertical $PM_{2.5}$ profiles from urban to suburban regions as this SBF moves northwest from Houston. Similar to the changes in the aerosol mass concentrations, the changes in the vertical distributions of nu0 (Fig. 10b) and ac0 number concentration (Fig. 10c) are not homogeneous within these layers. The cleaner air mass following the SBF replaces the higher aerosol number concentrations. However, the changes are not consistent throughout the vertical layers. The reduction in the concentrations is found over a larger spatial extent surrounding the M1 site. In addition, the changes in the number concentrations are slightly different for the two modes. The normalized changes in nu0 at the higher altitudes are >80% compared to ac0.

Overall, there is an interchange of low and high aerosol-laden air masses influenced by the inland propagating SBF. This pattern resembles that observed in SB simulations by Lu and Turco (1994), Verma et al. (2006), Igel et al. (2018), and Parajuli et al. (2022). Parajuli et al. (2022) observed that the SB pushes dust inland and upward along the mountain slopes, reaching heights of up to 1.5 km. During TRACER, the vertical influence of SAI extended up to ~1.5 km within PBLH. For TRACER, the region of SBC influence is shown to extend inland up to 50 km and vertically up to 2 km over a period of up to 5 hours following the passage of the SBF. The model simulations supplement the ARM TRACER observations by filling observational gaps and enabling the extrapolation of TRACER findings across a broader regional scale, an endeavor that would be challenging to achieve with limited in-situ observational sites or standalone models.

https://doi.org/10.5194/egusphere-2025-2659
Preprint. Discussion started: 27 June 2025

3.7 Impact of sea breeze aerosol interaction on aerosol direct and indirect effects

3.7.1 Changes in cloud condensation nuclei

Fig. 11a shows the time series of the normalized aerosol number concentration with Dp > 100 nm, N_{100} for the 10 July event. For this case, N_{100} serves as our proxy for the CCN concentration. Similar to the changes in the overall aerosol number budget, the SBF passage and the air mass that follows induces simultaneous changes in the CCN budget. During this event, the CCN concentration decreases by ~35% at M1 site and ~60% at S3 site, with these changes observed within an hour of the SBF passage. Simulations performed for this event also suggest similar changes in aerosol budget, indicating that the SBF brings in a cleaner air mass from directions consistent with a more marine environment. Model results suggest that the CCN concentration at the surface decreases by up to 60%, consistent with the observations.

In our supplemental Figs. S10. and S11., we include the temporal variation of the normalised N_{100} during all the other SB events during the TRACER IOP. The preexisting N_{100} is less frequently impacted by the SAI than previous examples we provided for SBF changes to the total number concentration, and these events show a decrease in N_{100} for ~25% of the SB events at both M1 and S3 site. This suggests that the influence of SAI is lesser over the marine influenced regional background aerosol larger than 100 nm in diameter.

3.7.2 Change in local Aerosol Radiative Forcing

Two model simulations, one including aerosol chemistry (WA) and one excluding it (NA), are used to estimate aerosol radiative forcing ARF over the southern Texas region. ARF (in Wm^{-2}) is defined as the change in Earth's energy balance due to the presence of aerosols in the atmosphere. Incorporating aerosol chemistry enables the model to account for interactions between anthropogenic and biogenic emissions and atmospheric processes, which are essential for accurately assessing ARF. We estimate ARM at three different levels: at the surface (ARF_{SUR}), in the atmosphere (ARF_{ATM}), and at the top of the atmosphere (ARF_{TOA}) using model simulated cloud-free incoming (F↓) and outgoing (F↑) radiation to isolate the direct impact of aerosols (following Subba et al., 2023):

https://doi.org/10.5194/egusphere-2025-2659
Preprint. Discussion started: 27 June 2025

$$ARF_{SUR/TOA} = (F\downarrow - F\uparrow)_{WA\_SUR/TOA} - (F\downarrow - F\uparrow)_{NA\_SUR/TOA} \quad (1)$$

$$ARF_{ATM} = ARF_{TOA} - ARF_{SUR} \quad (2)$$

The ARF_{ATM} is the difference between ARF_{SUR} and ARF_{TOA}, and reflects the cumulative aerosol forcing in the atmospheric column. In this study, ARF_{ATM} is used as a proxy for aerosol radiative effects over southern Texas during the SBF's influence. ARF_{ATM} signifies solar radiation trapped in the atmosphere, leading to atmospheric warming. Hourly ARF variations, influenced by the sea breeze, are calculated to assess their impact.

Fig. 12 shows the hourly ARF_{ATM} and their changes during the daytime SAI periods for our three case response scenarios. The ARF values before and after SBF passage are shown in columns 1 and 2, respectively. Column 3 presents the absolute change in ARF (after-before), and column 4 gives the normalized change. ARF_{ATM} fluctuates hourly in response to aerosol loading (Fig. 12). On 10 July ARF_{ATM} in Houston's urban core (around M1) had higher values (>15 W m^{-2}) compared to the surrounding regions (<6 W m^{-2}, around S3). Over the ocean, ARF_{ATM} values are lower and consistent with expectations for lower aerosol concentrations as discussed earlier. We have seen previously that the air mass preceding the SBF passage had lower aerosol concentrations, which then reduced the aerosol concentration at the site. After the SBF's passage, a reduction influence in aerosols led to a reduction in ARF_{ATM}, with the M1 site showing a decrease of ~-4.2 W m^{-2} (~35%).

The simulated output shows that during the enhanced influence case as on 17 July, the oceanic region showed slightly higher aerosol loading, with ARF_{ATM} values exceeding 12 W m^{-2} (Fig. 12b.). The M1 site experiences a positive change of ~+2.9 W m^{-2} (~18%) after SBF's passage. The increase in aerosol concentration caused greater perturbation of incoming solar radiation, reflected in the positive ARF_{ATM} change.

For the neutral influence case on 16 August, the ARF_{ATM} was lower over land than simulated for the other two days. The spatial distribution of ARF_{ATM} was similar between land and sea in these outputs. The absolute change in ARF_{ATM} around the M1 site was only ~ 1.0 W m^{-2} (~24%). This change is small relative to the overall ARF_{ATM} magnitude and more likely due to variability of the aerosol source and transportation rather than SAI.

It is important to remember that, like SAI, the ARF changes due to SAI are also localized. However, investigating ARF changes remains important, SAI tends to occur during periods of

https://doi.org/10.5194/egusphere-2025-2659
Preprint. Discussion started: 27 June 2025

both high solar radiation and high aerosol loading, conditions that can significantly impact regional ARF during SBC events. Looking across all the SB events having significant changes in aerosol loading, individual SBF's passage can alter local ARF_{ATM} by up to ±40% (±5 W m^{-2}) (Table S1). Since ARFs are estimates from simulations and not measured, quantifying changes due to aerosols and disentangling those changes due to aerosol meteorology interaction would be more challenging. This study presents an example of ARF changes driven by aerosol meteorology interaction over a small region but likely occurring along many coastlines globally. A detailed future study of the aerosol radiative forcing over the coastal region therefore warranted.

4 Summary and conclusions

Sea breezes influence multi-scale processes across the land-ocean-atmosphere interface within the region of influence of the SBC. The TRACER field campaign provided a unique opportunity to understand how aerosol and meteorological processes impact weather and climate in the urban and rural coastal environment of Houston, Texas. A total of 46 (M1) and 31 (S3) instances of SB passages were identified during the summertime TRACER IOP period. Summertime measurements from the ARM sites coupled with WRF-Chem model simulations (July and August 2022) help to quantify aerosol changes resulting from onshore transport of marine boundary layer air masses due to SBF passage and the associated atmospheric SBC impacts.

Understanding the spatial extent and duration of SAIs is crucial for assessing their environmental and meteorological impacts. For any inland-penetrating SBF, its influence on aerosols typically falls into one of the three types: reduction where the SB replaces polluted aerosol air with cleaner air; enhancement, where it introduces more polluted air; or neutral, where no significant change occurs because the air masses are similar. These impacts can vary depending on site proximity to the coast and the history of the air mass prior to SBF passage. TRACER measurements suggest that the urban M1 site (60% of SB days) closer to the land-ocean interface experiences more frequent changes in aerosol concentrations compared to the rural S3 site (34% of SB days) further downstream in this SBC region. Surface aerosol concentration during IOP events was observed to change by up to a factor of two, indicating significant variations in response to SAI. On average, SBF passages were associated with

https://doi.org/10.5194/egusphere-2025-2659
Preprint. Discussion started: 27 June 2025

aerosol number concentrations that decreased by ~25% at M1 and increased by ~7% at S3. These changes were accompanied by sudden shifts in meteorological conditions, including RH (+30%) and wind speed (+4 m s^{-1}) enhancements, and backing in wind directions to the southeast (Figs. 7. and 8.). The relationship between wind and aerosol number concentrations showed that aerosol concentrations at the M1 site are higher when prevailing winds originate from the direction of the Houston urban core (east to north), compared to the winds coming from the sea (south and intermediate directions) (Fig. S5).

WRF Chem simulations were performed to investigate the regional SAI influence for the gaps between TRACER ground sites, as well as to estimate ARFs that are not directly measurable. These outputs suggest that SBFs have heterogeneous spatial influence on the aerosol concentration (Figs. 10 and 11). The 18 TRACER events simulated indicate that surface $PM_{2.5}$ concentrations decrease by ~15% around the M1 site and increase by ~3% near the S3 site (Fig. S12). However, these responses vary with altitude (Fig. 10). For example, our efforts suggest the SBF may alter the vertical aerosol distribution in the boundary layer up to 2 km.

Coastal SBCs are a global phenomenon. Employing both TRACER observations and these targeted event simulations, we find that SAIs also modify the aerosol environment. In addition to bringing in cooler, moist air masses and promoting cloud formation in coastal regions, SBs also affect the local heating and cooling by modifying aerosol radiative effects. Both model simulations and IOP measurements indicate that the surface CCN concentrations decrease by up to 60% following SBF passage (Fig. 11). However, the change in CCN concentrations during SAI are rare (~25% of the SB events at both M1 and S3 site) suggesting a weaker impact of SAI on marine influenced regional background aerosols. Model simulations suggest that changes in the columnar distribution of the aerosols can lead to changes in the perturbation of the incoming solar radiation, resulting in changes in atmospheric aerosol radiative forcing by up to 40% over southern Texas (Fig. 12).

It is important to remember that these effects are localized, occurring only during shorter timescales (< 6 hours) associated with daily SBC cycles over these locations. But these SAI timings align with periods of peak solar radiation and elevated aerosol concentrations, potentially leading to significant impacts on radiation budget over the coastal regions. These effects vary based on site proximity to the land-water interface. The coastal environment contains a complex mixture of marine, terrestrial, and urban aerosols. SAI has a lesser impact on the marine-influenced background accumulation mode. The SB influences meteorological

https://doi.org/10.5194/egusphere-2025-2659
Preprint. Discussion started: 27 June 2025

conditions and the diurnal variability of aerosols, altering their direct and indirect radiative effects, which subsequently affect the aerosol environment. During times in close proximity to SBF passage, changes in solar radiation and cloud formation may influence the aerosol formation and distribution, modify atmospheric chemical reactions, and affect cloud formation and properties, thereby impacting various atmospheric processes and interactions. However, estimating changes in aerosol radiative forcing is challenging, therefore, a detailed future study of these changes across different coastal regions is important.

Code and data availability. DOE-ARM datasets can be downloaded from the ARM data discovery (https://adc.arm.gov//discovery/#/results/instrument_class_code::#). The TCEQ data can be downloaded from https://www.tceq.texas.gov/agency/data. The Weather Research and Forecasting Model with Chemistry model code is available from www2.mmm.ucar.edu/wrf/users/download/. WRF-Chem preprocessors are available on the website (www.acom.ucar.edu/wrf-chem). The model output data is made available upon request. The primary tools to analyze the model output and generate figures are CDO (code.mpimet.mpg.de/projects/cdo/), MATLAB (www.mathworks.com/products/), and Jupyter Notebook platform (https://jupyter.org).

Supplement. The supplementary document contains supplementary figures referred to in the main manuscript.

Author contribution. TS and CK planned the study; TS conducted the analysis and wrote the manuscript; MH provided the aerosol data; MJ, MD, SG, MH, AS, DW, MZ and CK reviewed and edited the manuscript.

Competing interests. The authors declare that they have no conflict of interest.

Acknowledgments. We would like to acknowledge support from the Atmospheric System Research (ASR) program, the Atmospheric Radiation Measurement (ARM) user facility, and the ARM TRACER operation and science teams. This research was supported in part by

https://doi.org/10.5194/egusphere-2025-2659
Preprint. Discussion started: 27 June 2025

resources provided by the National Energy Research Scientific Computing Center (NERSC), a DOE Office of Science User Facility under Contract No. DE-AC02-05CH11231, through NERSC award BER-ERCAP0026649. Additionally, the NE Linux Cluster (nlc) at Brookhaven National Laboratory was utilized for model simulations and output storage.

Financial support. This paper has been authored by employees of Brookhaven Science Associates, LLC, under Contract DE-SC0012704 with the U.S. Department of Energy (DOE).

References

Ackermann, I. J., Hass, H., Memmesheimer, M., Ebel, A., Binkowski, F. S., & Shankar, U.: Modal aerosol dynamics model for Europe: Development and first applications. Atmospheric Environment, 32(17), 2981–2999. https://doi.org/10.1016/S1352-2310(98)00006-5, 1998.

Adaricheva, K., Bernhardt, J. E., Liu, W., & Schmidt, B.: Importance of overnight parameters to predict Sea Breeze on Long Island. http://arxiv.org/abs/2309.01803, 2023.

Ahmadov, R., Gerbig, C., Kretschmer, R., Koerner, S., Neininger, B., Dolman, A. J., & Sarrat, C.: Mesoscale covariance of transport and CO2 fluxes: Evidence from observations and simulations using the WRF-VPRM coupled atmosphere-biosphere model. Journal of Geophysical Research Atmospheres, 112(22). https://doi.org/10.1029/2007JD008552, 2007.

Albrecht, B. A.: Aerosols, cloud microphysics, and fractional cloudiness. Science, 245, 1227–1230, 1989.

Aldhaif, A. M., Lopez, D. H., Dadashazar, H., & Sorooshian, A.: Sources, frequency, and chemical nature of dust events impacting the United States East Coast. Atmospheric Environment, 231. https://doi.org/10.1016/j.atmosenv.2020.117456, 2020.

Ariya, P., Sun, J., Eltouny, N., Hudson, E. D., Hayes, C. T., & Kos, G.: Physical and chemical characterization of bioaerosols—Implications for nucleation processes. International Reviews in Physical Chemistry, 28(1), 1–32. https://doi.org/10.1080/01442350802597438, 2009.

https://doi.org/10.5194/egusphere-2025-2659
Preprint. Discussion started: 27 June 2025

Arrillaga, J. A., Jiménez, P., de Arellano, J. V.-G., Jiménez, M. A., Román-Cascón, C., Sastre, M., and Yagüe, C.: Analyzing the synoptic-, meso- and local-scale involved in sea breeze formation and frontal characteristics. J. Geophys. Res. Atmos., 125, e2019JD031302, https://doi.org/10.1029/2019JD031302, 2020.

Atabakhsh, S., Poulain, L., Bigi, A., Coen, M. C., Pöhlker, M., & Herrmann, H.: Trends of PM1 aerosol chemical composition, carbonaceous aerosol, and source over the last 10 years at Melpitz (Germany). Atmospheric Environment, 346. https://doi.org/10.1016/j.atmosenv.2025.121075, 2025.

Augustin, P., Billet, S., Crumeyrolle, S., Deboudt, K., Dieudonné, E., Flament, P., Fourmentin, M., Guilbaud, S., Hanoune, B., Landkocz, Y., Méausoone, C., Roy, S., Schmitt, F. G., Sentchev, A., & Sokolov, A.: Impact of sea breeze dynamics on atmospheric pollutants and their toxicity in industrial and urban coastal environments. Remote Sensing, 12(4). https://doi.org/10.3390/rs12040648, 2020.

Banta, R. M., Senff, C. J., Alvarez, R. J., Langford, A. O., Parrish, D. D., Trainer, M. K., Darby, L. S., Michael Hardesty, R., Lambeth, B., Andrew Neuman, J., Angevine, W. M., Nielsen-Gammon, J., Sandberg, S. P., & White, A. B.: Dependence of daily peak O3 concentrations near Houston, Texas on environmental factors: Wind speed, temperature, and boundary-layer depth. Atmospheric Environment, 45(1), 162–173. https://doi.org/10.1016/j.atmosenv.2010.09.030, 2011.

Bao, S., Pietrafesa, L., Gayes, P., Noble, S., Viner, B., Qian, J. H., Werth, D., Mitchell, G., & Burdette, S.: Mapping the Spatial Footprint of Sea Breeze Winds in the Southeastern United States. Journal of Geophysical Research: Atmospheres, 128(7). https://doi.org/10.1029/2022JD037524, 2023.

Barrett, T. E., & Sheesley, R. J.: Urban impacts on regional carbonaceous aerosols: Case study in central Texas. Journal of the Air and Waste Management Association, 64(8), 917–926. https://doi.org/10.1080/10962247.2014.904252, 2014.

Bauman, W. H.: Verify MesoNAM Performance. NASA Contractor Report CR-2010-216-287, Kennedy Space Center, FL, 31 pp. [Available from ENSCO, Inc., 1980 N. Atlantic Ave., Suite 830, Cocoa Beach, FL, 32931 and online at http://science.ksc.nasa.gov/amu/final-reports/mesoNAMverify.pdf.], 2010.

https://doi.org/10.5194/egusphere-2025-2659
Preprint. Discussion started: 27 June 2025

Bond, T. C., Doherty, S. J., Fahey, D. W., Forster, P. M., Berntsen, T., Deangelo, B. J., Flanner, M. G., Ghan, S., Kärcher, B., Koch, D., Kinne, S., Kondo, Y., Quinn, P. K., Sarofim, M. C., Schultz, M. G., Schulz, M., Venkataraman, C., Zhang, H., Zhang, S., … Zender, C. S.: Bounding the role of black carbon in the climate system: A scientific assessment. Journal of Geophysical Research Atmospheres, 118(11), 5380–5552. https://doi.org/10.1002/jgrd.50171, 2013.

Borge, R., Alexandrov, V., José del Vas, J., Lumbreras, J., & Rodríguez, E.: A comprehensive sensitivity analysis of the WRF model for air quality applications over the Iberian Peninsula. Atmospheric Environment, 42(37), 8560–8574. https://doi.org/10.1016/j.atmosenv.2008.08.032, 2008.

Boyouk, N., Léon, J. F., Delbarre, H., Augustin, P., & Fourmentin, M.: Impact of sea breeze on vertical structure of aerosol optical properties in Dunkerque, France. Atmospheric Research, 101(4), 902–910. https://doi.org/10.1016/j.atmosres.2011.05.016, 2011.

Bozlaker, A., Prospero, J. M., Fraser, M. P., & Chellam, S.: Quantifying the contribution of long-range saharan dust transport on particulate matter concentrations in Houston, Texas, using detailed elemental analysis. Environmental Science and Technology, 47(18), 10179–10187. https://doi.org/10.1021/es4015663, 2013.

Brown, S., Nicholls, R. J., Woodroffe, C. D., Hanson, S., Hinkel, J., Kebede, A. S., Neumann, B. and Vafeidis, A. T.: “Sea-Level Rise Impacts and Responses: A Global Perspective.” In Coastal Hazards, edited by Charles W. Finkl, 117–49. Dordrecht: Springer Netherlands. https://doi. org/10.1007/978-94-007-5234-4_5, 2013.

Burkart, J., Gratzl, J., Seifried, T. M., Bieber, P., & Grothe, H.: Subpollen particles (SPP) of birch as carriers of ice nucleating macromolecules. Biogeosciences Discussions, 1–15, 2021.

Charlson, R. J., Schwartz, S. E., Hales, J. M., Cess, R. D., Coakley, J. A. Jr, Hansen, J. E., and Hofmann, D. J.: Climate forcing by anthropogenic aerosols. Science 255, 423—430, 1992.

Chen, F., & Dudhia, J.: Coupling an advanced land surface-hydrology model with the Penn State-NCAR MM5 modeling system. Part I: Model implementation and sensitivity. Monthly Weather Review, 129(4), 569–585. https://doi.org/10.1175/1520-0493(2001)129<0569:caalsh>2.0.co;2, 2001.

https://doi.org/10.5194/egusphere-2025-2659
Preprint. Discussion started: 27 June 2025

Chou, M., Suarez, M. J., Ho, C., Yan, M. M., & Lee, K.: Parameterizations for cloud overlapping and shortwave single-scattering properties for use in general circulation and cloud ensemble models. Journal of Climate, 11(2), 202–214. https://doi.org/10.1175/1520-0442(1998)011<0202:PFCOAS>2.0.CO;2, 1998.

Clappier, A., Martilli, A., Grossi, P., Thunis, P., Pasi, F., Krueger, B. C., Calpini, B., & Graziani, G., Bergh, H.V.D.: Effect of Sea Breeze on Air Pollution in the Greater Athens Area. Part I: Numerical Simulations and Field Observations. J. of Applied meteorology, (39). https://doi.org/10.1175/1520-0450(2000)039<0546:EOSBOA>2.0.CO;2, 1999.

Comin, A. N., Miglietta, M. M., Rizza, U., Acevedo, O. C., & Degrazia, G. A.: Investigation of sea-breeze convergence in Salento Peninsula (southeastern Italy). Atmospheric Research, 160, 68–79. https://doi.org/10.1016/j.atmosres.2015.03.010, 2015.

Crippa, M., Canonaco, F., Lanz, V. A., Äijälä, M., Allan, J. D., Carbone, S., Capes, G., Ceburnis, D., Dall'Osto, M., Day, D. A., DeCarlo, P. F., Ehn, M., Eriksson, A., Freney, E., Hildebrandt Ruiz, L., Hillamo, R., Jimenez, J. L., Junninen, H., KiendlerScharr, A., Kortelainen, A. M., Kulmala, M., Laaksonen, A., Mensah, A. A., Mohr, C., Nemitz, E., O'Dowd, C., Ovadnevaite, J., Pandis, S. N., Petäjä, T., Poulain, L., Saarikoski, S., Sellegri, K., Swietlicki, E., Tiitta, P., Worsnop, D. R., Baltensperger, U., Prévôt, A. S. H.: Organic aerosol components derived from 25 AMS data sets across Europe using a consistent ME-2 based source apportionment approach. Atmos. Chem. Phys. 14 (12), 6159–6176. https://doi.org/10.5194/acp-14-6159, 2014.

Crossett, K., Culliton, T., Wiley, P., & Goodspeed, T.: Population trends along the coastal United States, 1980–2008. Silver Spring, National Oceanic and Atmospheric Administration, 2004.

Das, S., Prospero, J. M., & Chellam, S.: Quantifying international and interstate contributions to primary ambient PM2.5 and PM10 in a complex metropolitan atmosphere. Atmospheric Environment, 292. https://doi.org/10.1016/j.atmosenv.2022.119415, 2023.

Deng, Min, et al.: A Closed Bay-Breeze Circulation and Its Lifecycle from TRACER with a New Orienteering Tape Recorder Diagram, Journal of Geophysical Research: Atmospheres (under revision), 2025.

https://doi.org/10.5194/egusphere-2025-2659
Preprint. Discussion started: 27 June 2025

di Bernardino, A., Iannarelli, A. M., Casadio, S., Mevi, G., Campanelli, M., Casasanta, G., Cede, A., Tiefengraber, M., Siani, A. M., Spinei, E., & Cacciani, M.: On the effect of sea breeze regime on aerosols and gases properties in the urban area of Rome, Italy. Urban Climate, 37. https://doi.org/10.1016/j.uclim.2021.100842, 2021.

Emmons, L. K., Walters, S., Hess, P. G., Lamarque, J. F., Pfister, G. G., Fillmore, D., et al.: Description and evaluation of the model for ozone and related chemical tracers, version 4 (MOZART-4). Geoscientific Model Development, 3(1), 43–67. https://doi.org/10.5194/gmd-3-43-2010, 2010.

Gangoiti, G., Millán, M. M., Salvador, R., & Mantilla, E.: Long-range transport and re-circulation of pollutants in the western Mediterranean during the project Regional Cycles of Air Pollution in the West-Central Mediterranean Area. Atmospheric Environment, 35(36), 6267–6276. https://doi.org/10.1016/S1352-2310(01)00440-X, 2001.

Georgiou, G. K., Christoudias, T., Proestos, Y., Kushta, J., Pikridas, M., Sciare, J., Savvides, C., & Lelieveld, J.: Evaluation of WRF-Chem model (v3.9.1.1) real-Time air quality forecasts over the Eastern Mediterranean. Geoscientific Model Development, 15(10), 4129–4146. https://doi.org/10.5194/gmd-15-4129-2022, 2022.

Grell, G. A., & Devenyi, D.: A generalized approach to parameterizing convection combining ensemble and data assimilation techniques. Geophysical Research Letters, 29(4), 38-1–38-4. https://doi.org/10.1029/2002GL015311, 2002.

Grell, G. A., Peckham, S. E., Schmitz, R., McKeen, S. A., Frost, G., Skamarock, W. C., & Eder, B.: Fully coupled “online” chemistry within the WRF model. Atmospheric Environment, 39(37), 6957–6975. https://doi.org/10.1016/j.atmosenv.2005.04.027, 2005.

Guenther, A. B., Jiang, X., Heald, C. L., Sakulyanontvittaya, T., Duhl, T., Emmons, L. K., & Wang, X.: The model of emissions of gases and aerosols from nature version 2.1 (MEGAN2.1): An extended and updated framework for modeling biogenic emissions. Geoscientific Model Development, 5(6), 1471–1492. https://doi.org/10.5194/gmd-5-1471-2012, 2012.

Hernández-Ceballos, M. A., Sorribas, M., San Miguel, E. G., Cinelli, G., Adame, J. A., & Bolívar, J. P.: Impact of sea-land breezes on 210Pb in southern Iberian Peninsula–

https://doi.org/10.5194/egusphere-2025-2659
Preprint. Discussion started: 27 June 2025

Feasibility study on using submicron-sized aerosol particles to analyze 210Pb hourly patterns. Atmospheric Pollution Research, 7(1), 1–8. https://doi.org/10.1016/j.apr.2015.06.011, 2016.

Hong, S. Y., Noh, Y., & Dudhia, J.: A new vertical diffusion package with an explicit treatment of entrainment processes. Monthly Weather Review, 134(9), 2318–2341. https://doi.org/10.1175/MWR3199.1, 2006.

Huang, X. F., He, L. Y., Hu, M., Canagaratna, M. R., Sun, Y., Zhang, Q., Zhu, T., Xue, L., Zeng, L. W., Liu, X. G., Zhang, Y. H., Jayne, J. T., Ng, N. L., Worsnop, D. R.: Highly time-resolved chemical characterization of atmospheric submicron particles during 2008 Beijing Olympic Games using an Aerodyne High-Resolution Aerosol Mass Spectrometer. Atmos. Chem. Phys. 2010, 10, 8933– 8945, DOI: 10.5194/acp-10-8933-2010.

Hudson, B.: Coastal Land Loss and the Mitigation-Adaptation Dilemma: Between Scylla and Charybdis Repository Citation Coastal Land Loss and the Mitigation-Adaptation Dilemma: Between Scylla and Charybdis. In Louisiana Law Review (Vol. 73). https://digitalcommons.law.lsu.edu/lalrev/vol73/iss1/3, 2012.

Igel, A. L., van den Heever, S. C., & Johnson, J. S.: Meteorological and Land Surface Properties Impacting Sea Breeze Extent and Aerosol Distribution in a Dry Environment. Journal of Geophysical Research: Atmospheres, 123(1), 22–37. https://doi.org/10.1002/2017JD027339, 2018.

IPCC, Intergovernmental Panel on Climate Change: In V. Masson-Delmotte, P. Zhai, A. Pirani, S. L. Connors, C. P.an, S. Berger, et al. (Eds.), The Physical Science Basis. Contribution of Working Group I to the Sixth Assessment Report of the Intergovernmental Panel on Climate Change. Cambridge University Press. https://doi.org/10.1017/9781009157896, 2021.

Iwai, H., Murayama, Y., Ishii, S., Mizutani, K., Ohno, Y., & Hashiguchi, T.: Strong Updraft at a Sea-Breeze Front and Associated Vertical Transport of Near-Surface Dense Aerosol Observed by Doppler Lidar and Ceilometer. Boundary-Layer Meteorology, 141(1), 117–142. https://doi.org/10.1007/s10546-011-9635-z, 2011.

Janjic, Z. I.: Nonsingular implementation of the Mellor–Yamada level 2.5 scheme in the NCEP Meso model. NCEP Office Note, 437, 61, 2002.

https://doi.org/10.5194/egusphere-2025-2659
Preprint. Discussion started: 27 June 2025

Jensen, M. P., and Coauthors, (2022): A Succession of Cloud, Precipitation, Aerosol, and Air Quality Field Experiments in the Coastal Urban Environment. Bull. Amer. Meteor. Soc., 103, 103–105, https://doi.org/10.1175/BAMS-D-21-0104.1, 2022.

Karnae, S., & John, K.: Source apportionment of PM2.5 measured in South Texas near U.S.A. – Mexico border. Atmospheric Pollution Research, 10(5), 1663–1676. https://doi.org/10.1016/j.apr.2019.06.007

Kerminen, V. M., Chen, X., Vakkari, V., Petäjä, T., Kulmala, M., & Bianchi, F. : Atmospheric new particle formation and growth: Review of field observations. In Environmental Research Letters (Vol. 13, Issue 10). Institute of Physics Publishing. https://doi.org/10.1088/1748-9326/aadf3c, 2018.

Kleinman, L. I., Daum, P. H., Imre, D. G., Lee, Y.-N., Nunnermacker, L. J., Springston, S. R., Weinstein-Lloyd, J., and Rudolph, J.: Ozone production rate and hydrocarbon reactivity in 5 urban areas: A cause of high ozone concentration in Houston, Geophys. Res. Lett., 29(10), 1467, doi:10.1029/2001GL014569, 2002.

Kuang, C., Chen, M., Zhao, J., Smith, J., McMurry, P. H., & Wang, J.: Size and time-resolved growth rate measurements of 1 to 5 nm freshly formed atmospheric nuclei. Atmospheric Chemistry and Physics, 12(7), 3573–3589. https://doi.org/10.5194/acp-12-3573-2012, 2012.

Kuang, C., McMurry, P. H., and McCormick, A. V.: Determination of cloud condensation nuclei production from measured new particle formation events, Geophys. Res. Lett., 36, L09822, doi:10.1029/2009GL037584, 2009.

Kulmala, M., Laakso, L., Lehtinen, K. E. J., Riipinen, I., Dal Maso, M., Anttila, T., Kerminen, V.-M., Horrak, U., Vana, M., and Tammet, H.: Initial steps of aerosol growth, Atmos. Chem. Phys., 4, 2553–2560, doi:10.5194/acp-4-2553-2004, 2004.

Kulmala, M., Petäjä, T., Ehn, M., Thornton, J., Sipilä, M., Worsnop, D. R., & Kerminen, V. M.: Chemistry of atmospheric nucleation: On the recent advances on precursor characterization and atmospheric cluster composition in connection with atmospheric new particle formation. Annual Review of Physical Chemistry, 65, 21–37. https://doi.org/10.1146/annurev-physchem-040412-110014, 2014.

https://doi.org/10.5194/egusphere-2025-2659
Preprint. Discussion started: 27 June 2025

Levy, M. E., Zhang, R., Khalizov, A. F., Zheng, J., Collins, D. R., Glen, C. R., Wang, Y., Yu, X. Y., Luke, W., Jayne, J. T., & Olaguer, E.: Measurements of submicron aerosols in Houston, Texas during the 2009 SHARP field campaign. Journal of Geophysical Research Atmospheres, 118(18), 10,518-10,534. https://doi.org/10.1002/jgrd.50785, 2013.

Li, W., Wang, Y., Bernier, C., & Estes, M.: Identification of Sea Breeze Recirculation and Its Effects on Ozone in Houston, TX, During DISCOVER-AQ 2013. Journal of Geophysical Research: Atmospheres, 125(22). https://doi.org/10.1029/2020JD033165, 2020.

Linden, P.F., Simpson, J.E., Gravity-driven flows in a turbulent fluid. Journal of Fluid Mechanics,172, 481-497. doi:10.1017/S0022112086001829, 1986.

Lu, R., & Turco, R. P.: Air pollutant transport in a coastal environment.1. 2-dimensional simulations of sea-breeze and mountain effects. Journal of the Atmospheric Sciences, 51(15), 2285–2308. https://doi.org/10.1175/1520-0469(1994)051<2285:APTIAC>2.0.CO;2, 1994.

Ma, S., & Tong, D. Q.: Neighborhood Emission Mapping Operation (NEMO): A 1-km anthropogenic emission dataset in the United States. Scientific Data, 9(1). https://doi.org/10.1038/s41597-022-01790-9, 2022.

Mack, S. M., Madl, A. K., & Pinkerton, K. E.: Respiratory health effects of exposure to ambient particulate matter and bioaerosols. Comprehensive Physiology, 10(1), 1–20. https://doi.org/10.1002/cphy.c180040, 2020.

Mao, F., Zang, L., Wang, Z., Pan, Z., Zhu, B., & Gong, W.: Dominant synoptic patterns during wintertime and their impacts on aerosol pollution in Central China. Atmospheric Research, 232. https://doi.org/10.1016/j.atmosres.2019.104701, 2020.

Masselink, G., and Pattiaratchi, C. B.: The effect of sea breeze on beach morphology, surf zone hydrodynamics and sediment resuspension, Mar. Geol., 146, 115–135, 1998.

Mather, J. H., and Voyles, J. W.: The Arm Climate Research Facility: A Review of Structure and Capabilities. Bull. Amer. Meteor. Soc., 94, 377–392, https://doi.org/10.1175/BAMS-D-11-00218.1, 2013.

https://doi.org/10.5194/egusphere-2025-2659
Preprint. Discussion started: 27 June 2025

Miller, S. T. K., Keim, B. D., Talbot, R. W., & Mao, H.: Sea breeze: Structure, forecasting, and impacts. Reviews of Geophysics, 41(3). https://doi.org/10.1029/2003RG000124, 2003.

Minguillón, M. C., Ripoll, A., Pérez, N., Prévôt, A. S. H., Canonaco, F., Querol, X., and Alastuey, A.: Chemical characterization of submicron regional background aerosols in the western Mediterranean using an Aerosol Chemical Speciation Monitor, Atmos. Chem. Phys., 15, 6379–6391, https://doi.org/10.5194/acp-15-6379-2015, 2015.

Mlawer, E. J., Taubman, S. J., Brown, P. D., Iacono, M., & Clough, S. A.: Radiative transfer for inhomogeneous atmospheres: RRTM, a validated correlated-k model for the longwave. Journal of Geophysical Research, 102(D14), 16663–16682. https://doi.org/10.1029/97JD00237, 1997.

Monin, A. S., & Obukhov, A. M.: Basic laws of turbulent mixing in the surface layer of the atmosphere. Contributions of the Geophysical Institute of the Slovak Academy of Science, USSR, 151, 163–187, 1954.

Moorthy, K. K., Murthy, B. V. K., and Nair, P. R.: Sea-breeze front effects on boundary layer aerosols at a tropical station, J. Appl. Meteorol., 32, 1196–1205. 1993.

Moorthy, K. K., Pillai, P. S., & Suresh Babu, S.: Influence of changes in the prevailing synoptic conditions on the response of aerosol characteristics to land-and sea-breeze circulations at a coastal station. In Boundary-Layer Meteorology (Vol. 108), 2003.

Morrison, H., Curry, J. A., and Khvorostyanov, V. I.: A new double-moment microphysics parameterization for application in cloud and climate models. Part I: Description. Journal of the Atmospheric Sciences, 62(6), 1665–1677. https://doi.org/10.1175/jas3446.1, 2005.

Papanastasiou, D. K., Melas, D., Bartzanas, T., & Kittas, C.: Temperature, comfort and pollution levels during heat waves and the role of sea breeze. International Journal of Biometeorology, 54(3), 307–317. https://doi.org/10.1007/s00484-009-0281-9, 2010.

Parajuli, S. P., Stenchikov, G. L., Ukhov, A., Mostamandi, S., Kucera, P. A., Axisa, D., Gustafson, W. I., & Zhu, Y.: Effect of dust on rainfall over the Red Sea coast based on WRF-Chem model simulations. Atmospheric Chemistry and Physics, 22(13), 8659–8682. https://doi.org/10.5194/acp-22-8659-2022, 2022.

https://doi.org/10.5194/egusphere-2025-2659
Preprint. Discussion started: 27 June 2025

Parajuli, S., Stenchikov, G. G., Ukhov, A., Shevchenko, I., Dubovik, O., & Lopatin, A.: Aerosol vertical distribution and interactions with land/sea breezes over the eastern coast of the Red Sea from lidar data and high-resolution WRF-Chem simulations. Atmospheric Chemistry and Physics, 20(24), 16089–16116. https://doi.org/10.5194/acp-20-16089-2020, 2020.

Park, J. M., van den Heever, S. C., Igel, A. L., Grant, L. D., Johnson, J. S., Saleeby, S. M., Miller, S. D., & Reid, J. S. (2020). Environmental Controls on Tropical Sea Breeze Convection and Resulting Aerosol Redistribution. Journal of Geophysical Research: Atmospheres, 125(6). https://doi.org/10.1029/2019JD031699, 2020.

Park, M. J., and van den Heever, S. C.: Weakening of tropical sea breeze convective systems through interactions of aerosol, radiation, and soil moisture. Atmospheric Chemistry and Physics, 22(16), 10527–10549. https://doi.org/10.5194/acp-22-10527-2022, 2022.

Parrish, D. D., Allen, D. T., Bates, T. S., Estes, M., Fehsenfeld, F. C., Feingold, G., Ferrare, R., Hardesty, R. M., Meagher, J. F., Nielsen-Gammon, J. W., Pierce, R. B., Ryerson, T. B., Seinfeld, J. H., & Williams, E. J.: Overview of the second texas air quality study (TexAQS II) and the Gulf of Mexico atmospheric composition and climate study (GoMACCS). Journal of Geophysical Research Atmospheres, 114(13). https://doi.org/10.1029/2009JD011842, 2009.

Partanen, A. I., Landry, J. S., and Matthews, H. D.: Climate and health implications of future aerosol emission scenarios. Environmental Research Letters, 13(2). https://doi.org/10.1088/1748-9326/aaa511, 2018.

Perry, K. D., Cahill, T. A., Eldred, R. A., Dutcher, D. D., and Gill, T. E.: Long-range transport of North African dust to the eastern United States. Journal of Geophysical Research Atmospheres, 102(10), 11225–11238. https://doi.org/10.1029/97jd00260, 1997.

Pinto, J. P., Dibb, J., Lee, B. H., Rappenglück, B., Wood, E. C., Levy, M., Zhang, R. Y., Lefer, B., Ren, X. R., Stutz, J., Tsai, C., Ackermann, L., Golovko, J., Herndon, S. C., Oakes, M., Meng, Q. Y., Munger, J. W., Zahniser, M., & Zheng, J.: Intercomparison of field measurements of nitrous acid (HONO) during the SHARP campaign. Journal of Geophysical Research, 119(9), 5583–5601. https://doi.org/10.1002/2013JD020287, 2014.

https://doi.org/10.5194/egusphere-2025-2659
Preprint. Discussion started: 27 June 2025

Plant, R. S., & Keith, G. J.: Occurrence of Kelvin-Helmholtz billows in sea-breeze circulations. Boundary-Layer Meteorology, 122(1), 1–15. https://doi.org/10.1007/s10546-006-9089-x, 2007.

Qi, L., Vogel, A. L., Esmaeilirad, S., Cao, L., Zheng, J., Jaffrezo, J. L., Fermo, P., Kasper-Giebl, A., Daellenbach, K. R., Chen, M., Ge, X., Baltensperger, U., Prévôt, A. S. H., & Slowik, J. G.: A 1-year characterization of organic aerosol composition and sources using an extractive electrospray ionization time-of-flight mass spectrometer (EESI-TOF). Atmospheric Chemistry and Physics, 20(13), 7875–7893. https://doi.org/10.5194/acp-20-7875-2020, 2020.

Ramanathan, V., Crutzen, P. J., Kiehl, J. T., & Rosenfeld, D.: Aerosols, Climate, and the Hydrological Cycle. Science, 294, 5549, DOI: 10.1126/science.1064034, 2001.

Rao, P. A., & Fuelberg, H. E.: An Investigation of Convection behind the Cape Canaveral Sea-Breeze Front, 2000.

Rosenfeld, D., et al.: Flood or drought: How do aerosols affect precipitation? Science, 321, 1309–1313, 2008.

Ryerson, T. B., Trainer, M., Angevine, W. M., Brock, C. A., Dissly, R. W., Fehsenfeld, F. C., Frost, G. J., Goldan, P. D., Holloway, J. S., Hübler, G., Jakoubek, R. O., Kuster, W. C., Neuman, J. A., Nicks, D. K., Parrish, D. D., Roberts, J. M., Sueper, D. T., Atlas, E. L., Donnelly, S. G., et al.: Effect of petrochemical industrial emissions of reactive alkenes and NOx on tropospheric ozone formation in Houston, Texas. Journal of Geophysical Research: Atmospheres, 108(8). https://doi.org/10.1029/2002jd003070, 2003.

Schell, B., Ackerman, I. J., Hass, H., Binkowski, F. S., & Ebel, A.: Modelling the formation of secondary organic aerosol within a comprehensive air quality model system. Journal of Geophysical Research, 106(D22), 28275–28293. https://doi.org/10.1029/2001JD000384, 2001.

Shrestha, S., Zhou, S., Mehra, M., Guagenti, M., Yoon, S., Alvarez, S. L., Guo, F., Chao, C. Y., Flynn, J. H., Wang, Y., Griffin, R. J., Usenko, S., & Sheesley, R. J.: Evaluation of aerosol- and gas-phase tracers for identification of transported biomass burning emissions in an industrially influenced location in Texas, USA. Atmospheric Chemistry and Physics, 23(19), 10845–10867. https://doi.org/10.5194/acp-23-10845-2023, 2023.

https://doi.org/10.5194/egusphere-2025-2659
Preprint. Discussion started: 27 June 2025

Simpson, J. E.: Sea Breeze and Local Wind, 234 pp., Cambridge Univ. Press, New York, 1994.

Singh, A. and Kuang, C.: Scanning Mobility Particle Sizer (SMPS) Instrument Handbook. U.S. Department of Energy, Atmospheric Radiation Measurement user facility, Richland, Washington. DOE/SC-ARM-TR-147, 2024.

Skamarock, W. C., Klemp, J. B., Dudhia, J., Gill, D. O., Barker, D., Wang, W., Powers, J. G.: A description of the Advanced Research WRF version 3. NCAR Tech. Note NCAR/TN-475+STR, 113 pp., doi:10.5065/D68S4MVH, 2008.

Song, S. K., Choi, Y. N., Choi, Y., Flynn, J., & Sadeghi, B.: Characteristics of aerosol chemical components and their impacts on direct radiative forcing at urban and suburban locations in Southeast Texas. Atmospheric Environment, 246. https://doi.org/10.1016/j.atmosenv.2020.118151, 2021.

Soni, M., Verma, S., Mishra, M. K., Mall, R. K., and Payra, S.: Estimation of particulate matter pollution using WRF-Chem during dust storm event over India. Urban Climate, 44. https://doi.org/10.1016/j.uclim.2022.101202, 2022.

Stockwell, W. R., Middleton, P., Chang, J. S., and Tang, X.: The second generation regional acid deposition model chemical mechanism for regional air quality modeling. Journal of Geophysical Research, 95(D10), 16343–16367. https://doi.org/10.1029/JD095iD10p16343, 1990.

Subba, T., Pathak, B., Gogoi, M. M., Ajay, P., Dahutia, P., Chakraborty, A., & Bhuyan, P. K.: Observations on the decadal variability of aerosol in eastern Himalayan foothills: Evidence of an anthropologically induced positive shift. Atmospheric Environment, 299. https://doi.org/10.1016/j.atmosenv.2023.119638, 2023.

Talbot, C., Augustin, P., Leroy, C., Willart, V., Delbarre, H., Khomenko, G.: Impact of a sea breeze on the boundary-layer dynamics and the atmospheric stratification in a coastal area of the North Sea. BoundaryLayer Meteorology, 125, 133–154, 2007.

Tuccella, P., Curci, G., Visconti, G., Bessagnet, B., Menut, L., & Park, R. J.: Modeling of gas and aerosol with WRF/Chem over Europe: Evaluation and sensitivity study. Journal of Geophysical Research Atmospheres, 117(3). https://doi.org/10.1029/2011JD016302, 2012.

Twomey, S.: Pollution and the planetary albedo. Atmos. Environ., 8, 1251–1256, 1974.

https://doi.org/10.5194/egusphere-2025-2659
Preprint. Discussion started: 27 June 2025

Uin, J., Aiken, A. C., Dubey, M. K., Kuang, C., Pekour, M., Salwen, C., Sedlacek, A. J., Senum, G., Smith, S., Wang, J., Watson, T. B., & Springston, S. R.: Atmospheric radiation measurement (ARM) aerosol observing systems (AOS) for surface-based in situ atmospheric aerosol and trace gas measurements. Journal of Atmospheric and Oceanic Technology, 36(12), 2429–2447. https://doi.org/10.1175/JTECH-D-19-0077.1, 2019.

Verma, S., Boucher, O., Venkataraman, C., Reddy, M. S., Müller, D., Chazette, P., & Crouzille, B.: Aerosol lofting from sea breeze during the Indian Ocean Experiment. Journal of Geophysical Research, 111, 07208. https://doi.org/10.1029/2005JD005953 , 2006.

Viner, B., Noble, S., Qian, J. H., Werth, D., Gayes, P., Pietrafesa, L., and Bao, S.: Frequency and characteristics of inland advecting sea breezes in the Southeast United States. Atmosphere, 12(8). https://doi.org/10.3390/atmos12080950, 2021.

Wang, B., Geddes, J. A., Adams, T. J., Lind, E. S., McDonald, B. C., He, J., Harkins, C., Li, D., and Pfister, G. G.: Implications of Sea Breezes on Air Quality Monitoring in a Coastal Urban Environment: Evidence From High Resolution Modeling of NO2 and O3. Journal of Geophysical Research: Atmospheres, 128(11). https://doi.org/10.1029/2022jd037860, 2023.

Wang, D., Jensen, M. P., Taylor, D., Kowalski, G., Hogan, M., Wittemann, B. M., Rakotoarivony, A., Giangrande, S. E., & Park, J. M.: Linking Synoptic Patterns to Cloud Properties and Local Circulations Over Southeastern Texas. Journal of Geophysical Research: Atmospheres, 127(5). https://doi.org/10.1029/2021JD035920, 2022.

Wang, D., Melvin, E. C., Smith, N., Jensen, M. P., Gupta, S., Abdullah-Smoot, A., Pszeniczny, N., & Hahn, T.: TRACER Perspectives on Gulf-Breeze and Bay-Breeze Circulations and Coastal Convection. Monthly Weather Review, 152(10), 2207–2228. https://doi.org/10.1175/MWR-D-23-0292.1, 2024.

Wang, S. C., Wang, Y., Estes, M., Lei, R., Talbot, R., Zhu, L., & Hou, P.: Transport of Central American Fire Emissions to the U.S. Gulf Coast: Climatological Pathways and Impacts on Ozone and PM2.5. Journal of Geophysical Research: Atmospheres, 123(15), 8344–8361. https://doi.org/10.1029/2018JD028684, 2018.

https://doi.org/10.5194/egusphere-2025-2659
Preprint. Discussion started: 27 June 2025

Watson, TB.: Aerosol Chemical Speciation Monitor (ACSM) Instrument Handbook. U.S. Department of Energy, Atmospheric Radiation Measurement user facility, Richland, Washington.DOE/SC-ARM-TR-196, 2024.

Wert, B. P., Trainer, M., Fried, A., Ryerson, T. B., Henry, B., Potter, W., Angevine, W. M., Atlas, E., Donnelly, S. G., Fehsenfeld, F. C., Frost, G. J., Goldan, P. D., Hansel, A., Holloway, J. S., Hubler, G., Kuster, W. C., Nicks, D. K., Neuman, J. A., Parrish, D. D., … Wisthaler, A.: Signatures of terminal alkene oxidation in airbone formaldehyde measurements during TexAQS 2000. Journal of Geophysical Research D: Atmospheres, 108(3). https://doi.org/10.1029/2002jd002502, 2003.

Westenbarger, D. A., & Morris, G. A.: Identifying biomass burning impacts on air quality in Southeast Texas 26–29 August 2011 using satellites, models and surface data. https://doi.org/10.5194/acp-2017-1234, 2018.

Yoon, S., Ortiz, S. M., Clark, A. E., Barrett, T. E., Usenko, S., Duvall, R. M., Ruiz, L. H., Bean, J. K., Faxon, C. B., Flynn, J. H., Lefer, B. L., Leong, Y. J., Griffin, R. J., & Sheesley, R. J.: Apportioned primary and secondary organic aerosol during pollution events of DISCOVER-AQ Houston. Atmospheric Environment, 244. https://doi.org/10.1016/j.atmosenv.2020.117954, 2021.

https://doi.org/10.5194/egusphere-2025-2659
Preprint. Discussion started: 27 June 2025

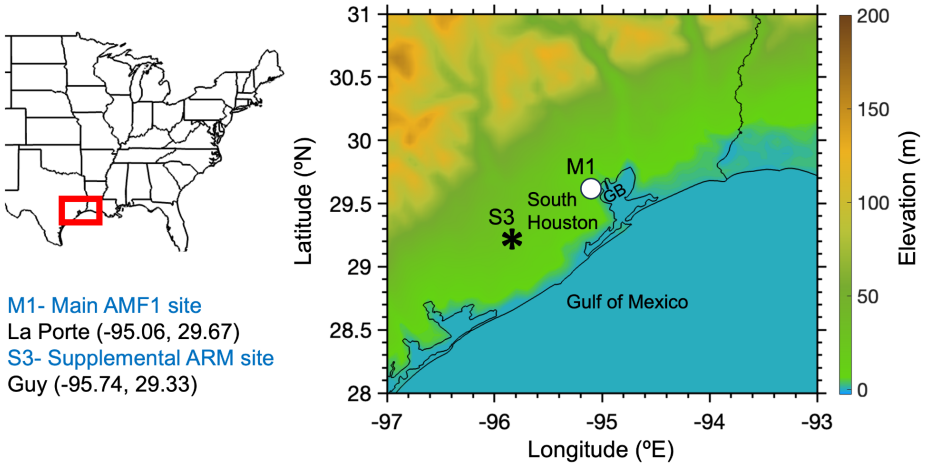

Figure 1. Map showing the TRACER field campaign main site (M1) and supplemental site (S3). Terrain elevation is shown in color. Here, "GB" corresponds to the Galveston Bay.

https://doi.org/10.5194/egusphere-2025-2659
Preprint. Discussion started: 27 June 2025

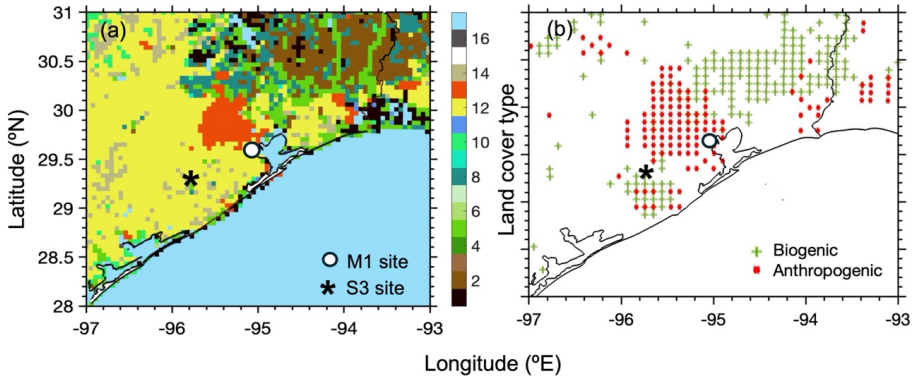

Figure 2. Weather Research and Forecasting model coupled with Chemistry (WRF-Chem) simulation domain with (a) primary land cover types comprising of (1) Evergreen Needleleaf Forest, (2) Evergreen Broadleaf Forest, (3) Deciduous Needleleaf Forest, (4) Deciduous Broadleaf Forest, (5) Mixed Forest, (6) Closed Shrubland, (7) Open Shrubland, (8) Woody Savanna, (9) Savanna, (10) Grassland, (11) Permanent Wetlands, (12) Cropland, (13) Urban and Build-up, (14) Cropland/Natural Mosaic, (15) Snow and Ice, (16) Barren or Sparsely Vegetated, and (17) Water; (b) Anthropogenic (red dots) and biogenic (green dots) aerosol emission source points obtained using the National Emissions Inventory (NEI) data and Model of Emissions of Gases and Aerosols from Nature (MEGAN) modeling system, respectively.

https://doi.org/10.5194/egusphere-2025-2659
Preprint. Discussion started: 27 June 2025

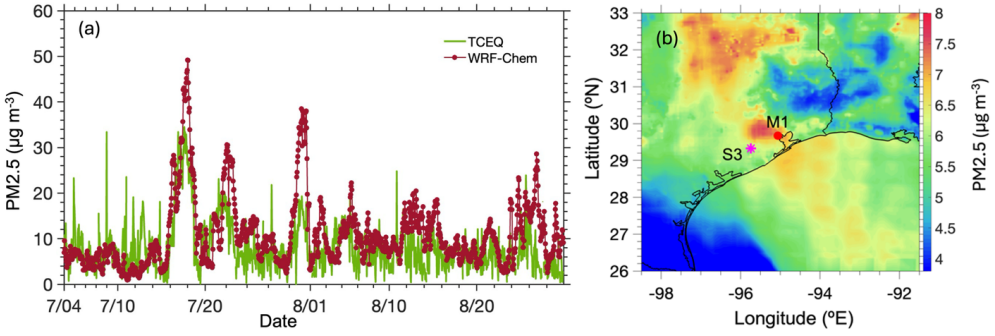

Figure 3. (a) Comparison of daily averaged $PM_{2.5}$ observed (green) at the TCEQ site, and WRF-Chem simulated (red) at the M1 site. (b) Spatial distribution of averaged $PM_{2.5}$ simulated with WRF-chem (color-filled contour).

https://doi.org/10.5194/egusphere-2025-2659
Preprint. Discussion started: 27 June 2025

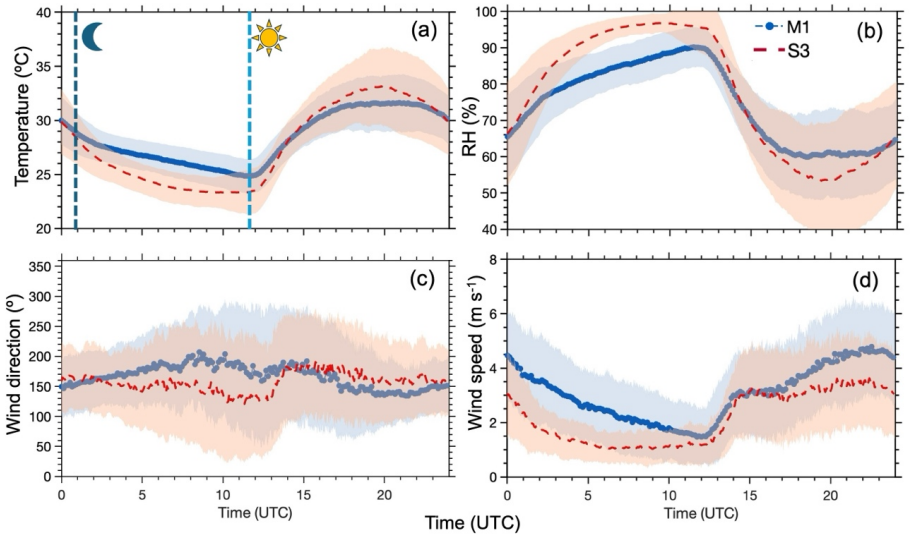

Figure 4. Diurnal variation of meteorological variables (a) Temperature at 2 m, (b) relative humidity (RH) (c) wind speed at 10 m, and (d) wind direction at 10 m measured at M1 (in blue) and S3 (in orange) sites averaged during IOP. The shaded color represents the standard deviation from the mean.

https://doi.org/10.5194/egusphere-2025-2659
Preprint. Discussion started: 27 June 2025

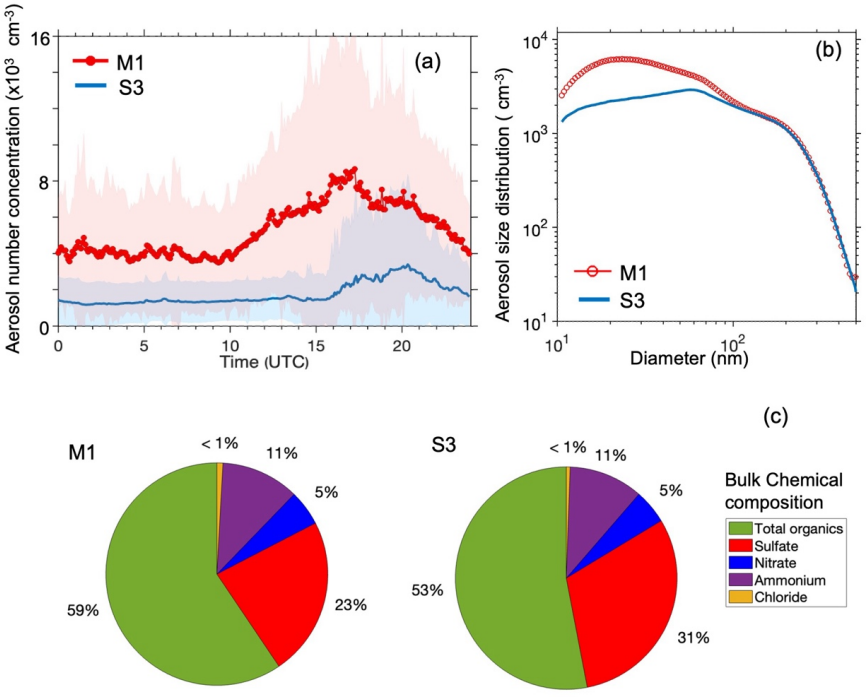

Figure 5. Measured (a) diurnal distribution of aerosol number concentration, (b) aerosol size distribution, and (c) percentage contribution of bulk chemical composition at M1 and S3 sites averaged from June to September 2022.

https://doi.org/10.5194/egusphere-2025-2659
Preprint. Discussion started: 27 June 2025

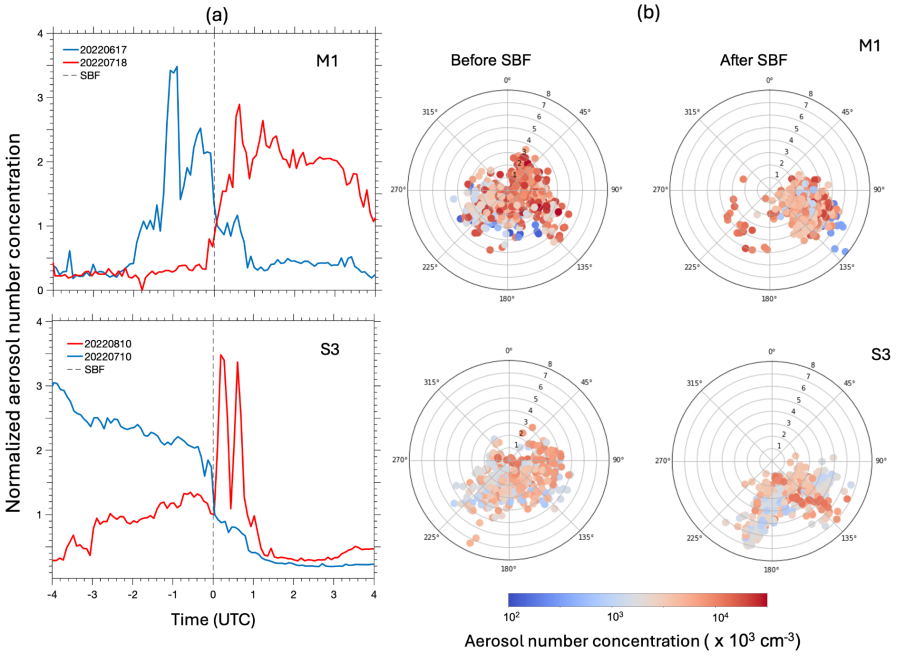

Figure 6. (a) Time series of the normalized aerosol number concentration, with the time centered at the time of the passing of the SBF (T_{SBF}=0) at the M1 site (first row) and the S3 site (second row) during the individual SB event days. (b) Open-air polar plots for aerosol number concentration before and after the passing of the SBF ($\Delta T = T_{SBF} \pm 1$). The wind speed (in m s^{-1}) grid lines are presented with black circles; the color scales represent the concentrations observed with each wind speed and direction combinations during the SB event days in June-September 2022.

https://doi.org/10.5194/egusphere-2025-2659
Preprint. Discussion started: 27 June 2025

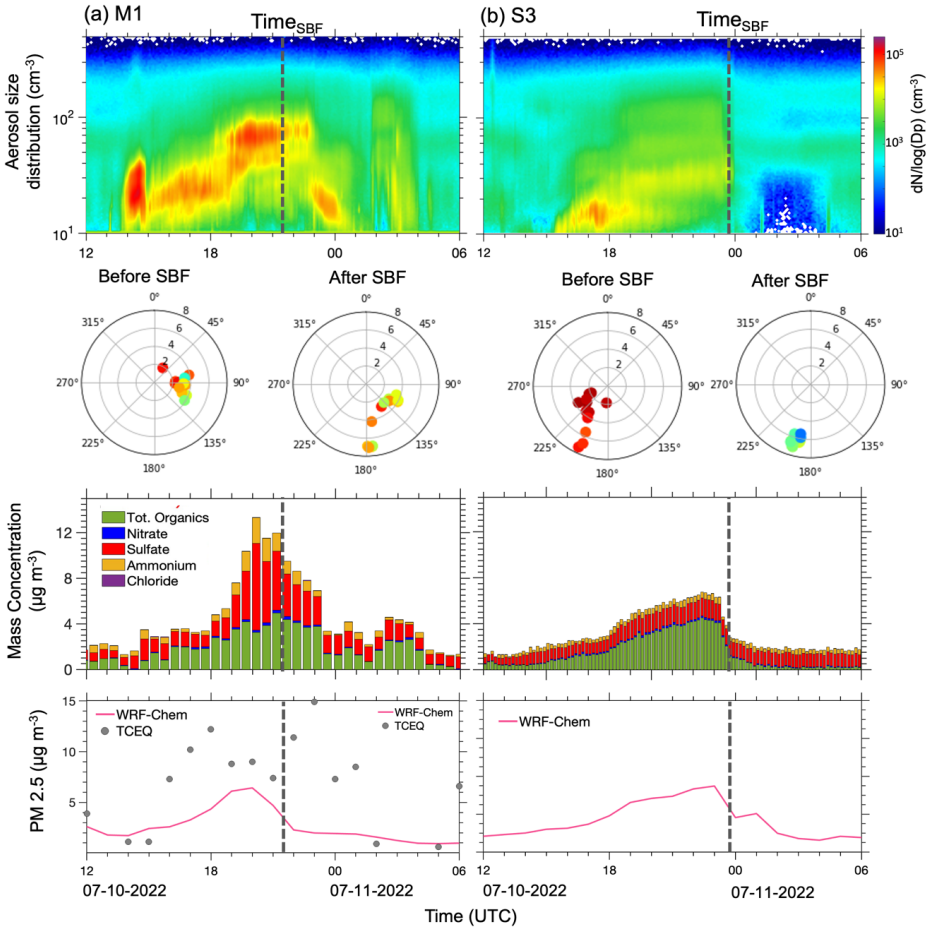

Figure 7. Time series of measured aerosol size distribution, measured bulk chemical composition, and modeled and TCEQ measured $PM_{2.5}$ mass concentration at (a) M1 and (b) S3 on 10 July 2022. Polar plot showing the measured integrated aerosol number concentration during one hour before and after the passing of the SBF. The black dashed line represents the time of the passing of the SBF (T_{SBF}) at the respective sites.

https://doi.org/10.5194/egusphere-2025-2659
Preprint. Discussion started: 27 June 2025

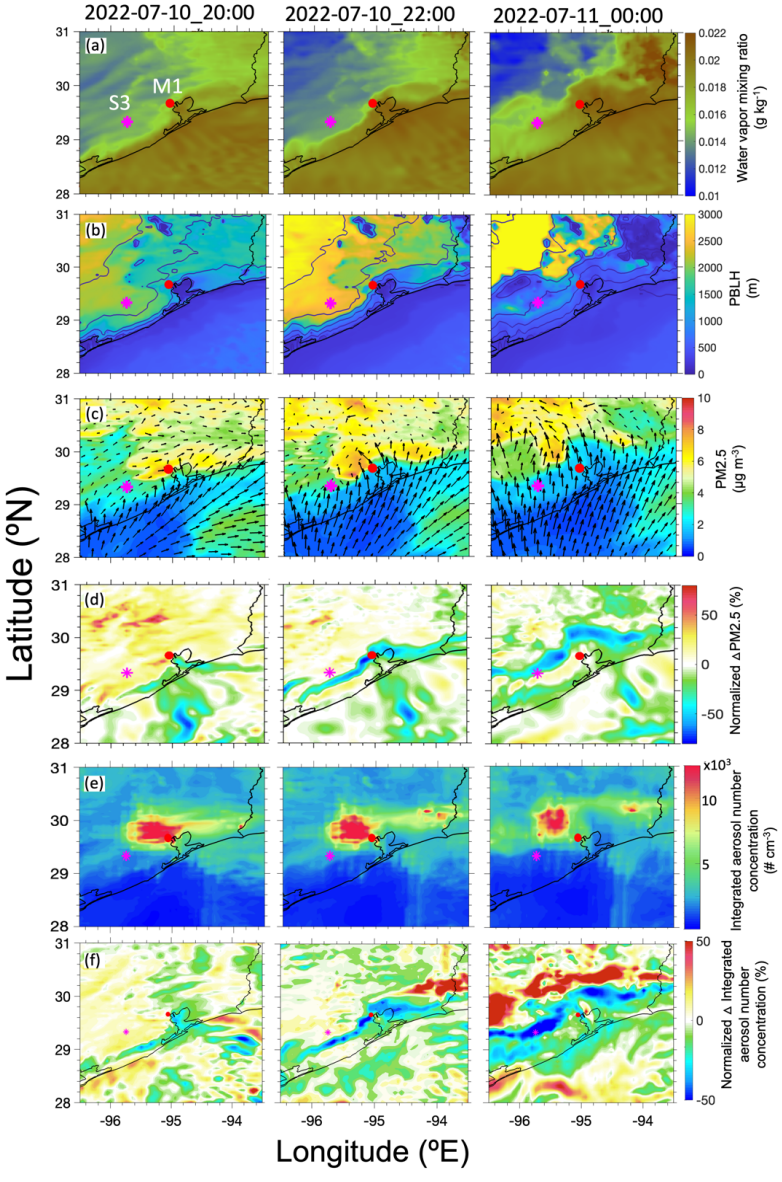

Figure 8. Modeled surface distribution of (a) water vapor mixing ratio, (b) PBLH, (c) $PM_{2.5}$, and wind vector (black arrows, at the surface), and (e) integrated aerosol number concentration (nucleation + accumulation mode) at three-time steps: 20:00 and 22:00 UTC on 10 July, and 00:00 UTC on 11 July. Sub-panels (d) and (f) show the normalized changes, where Δ is the change from the previous time step.

https://doi.org/10.5194/egusphere-2025-2659
Preprint. Discussion started: 27 June 2025

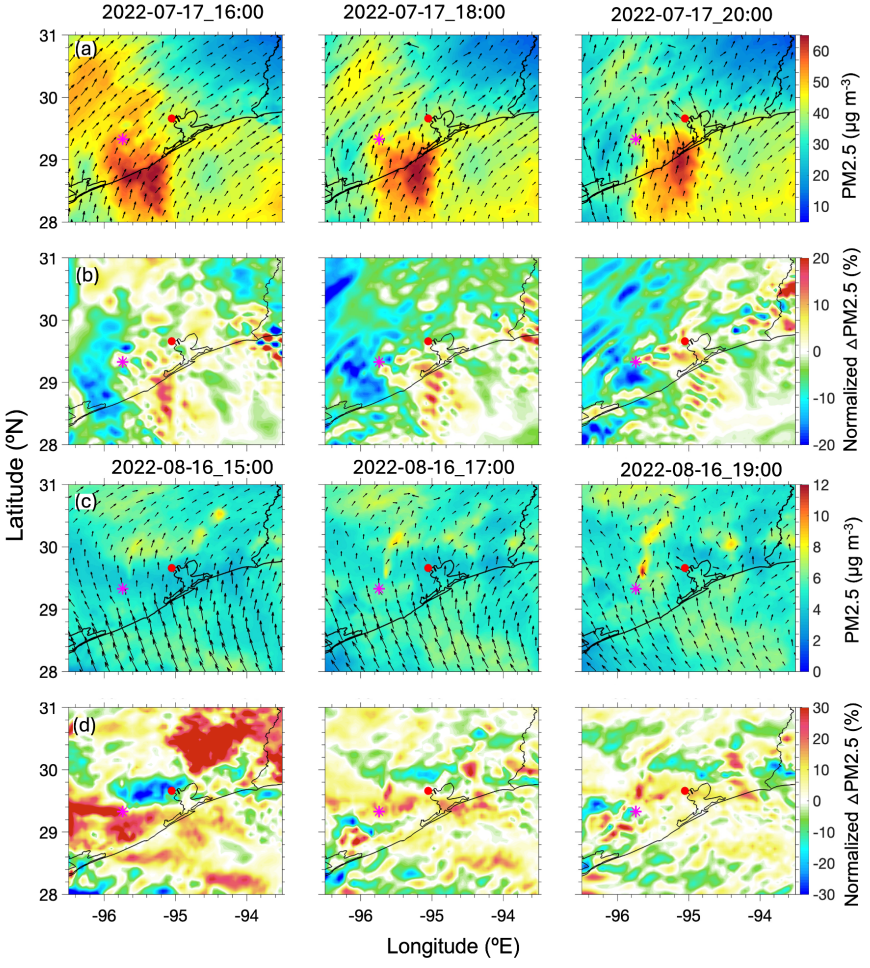

Figure 9. Modeled surface distribution of (a) $PM_{2.5}$ on 17 July and (c) 16 August at the respective hours as shown in the panels. Sub-panels (b) and (d) show the normalized changes, where Δ is the change from the previous time step. The filled-circle marker in the panels represents the M1 site, while the star represents the S3 site.

https://doi.org/10.5194/egusphere-2025-2659
Preprint. Discussion started: 27 June 2025

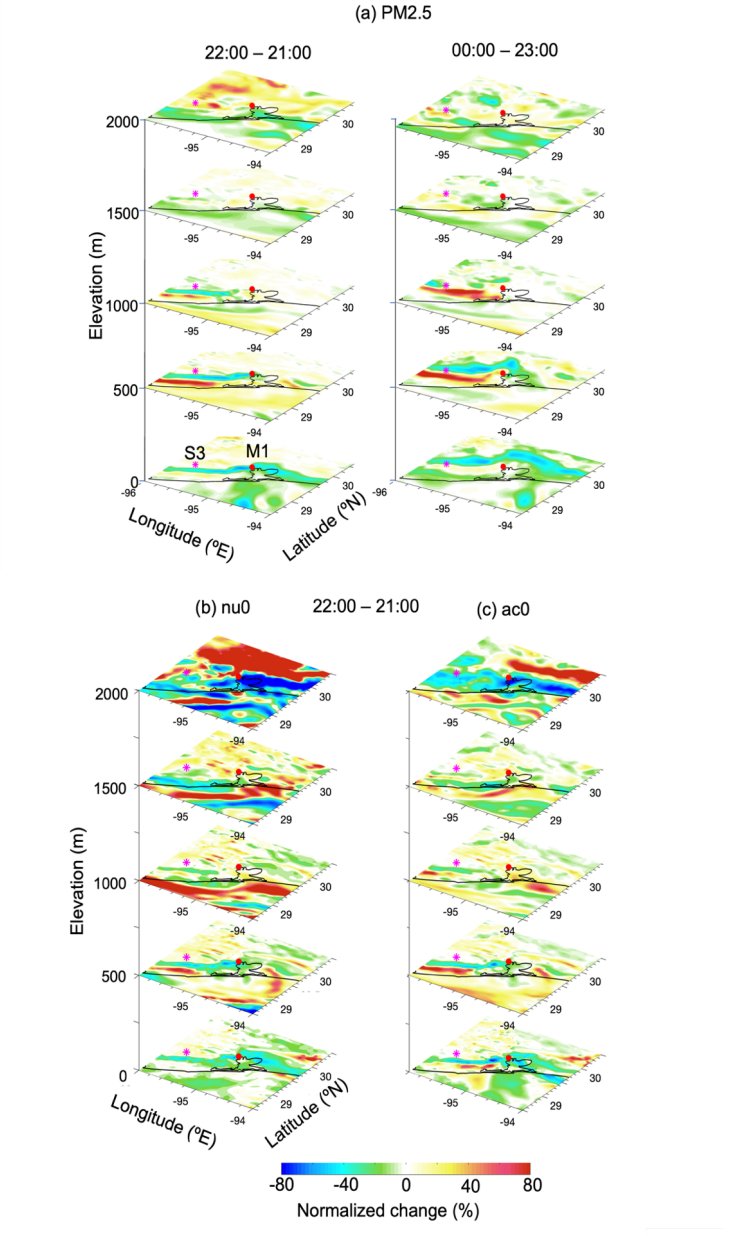

Figure 10. First row: the spatial distribution of normalised $\Delta PM_{2.5}$ at different elevations at timesteps (a) 21:00 and 22:00 UTC on 10 July, and 23:00 UTC on 10 July and 00:00 UTC on 11 July. Second row: the spatial distribution of normalised (b) Δnucleation mode (nu0) and (c) Δaccumulation mode (ac0) aerosol number concentration at timesteps 21:00 and 22:00 UTC on 10 July.

https://doi.org/10.5194/egusphere-2025-2659
Preprint. Discussion started: 27 June 2025

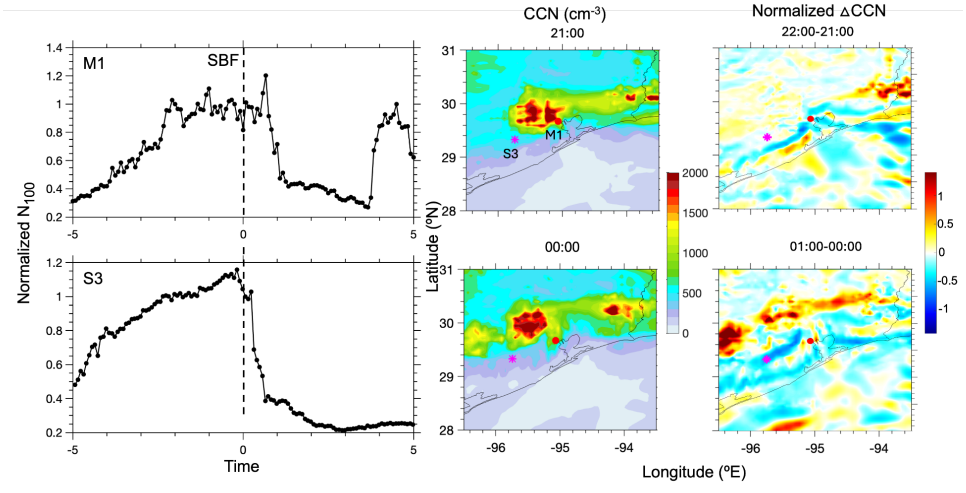

Figure 11. Time series of the normalized measured N_{100} along the time normalised to the time of the SBF's passing through the M1 site (first row) and the S3 site (second row) on 10 July 2022 (1st column). Spatial distribution of the modeled hourly averaged (2nd column) and normalized ΔCCN (3rd column).

https://doi.org/10.5194/egusphere-2025-2659
Preprint. Discussion started: 27 June 2025

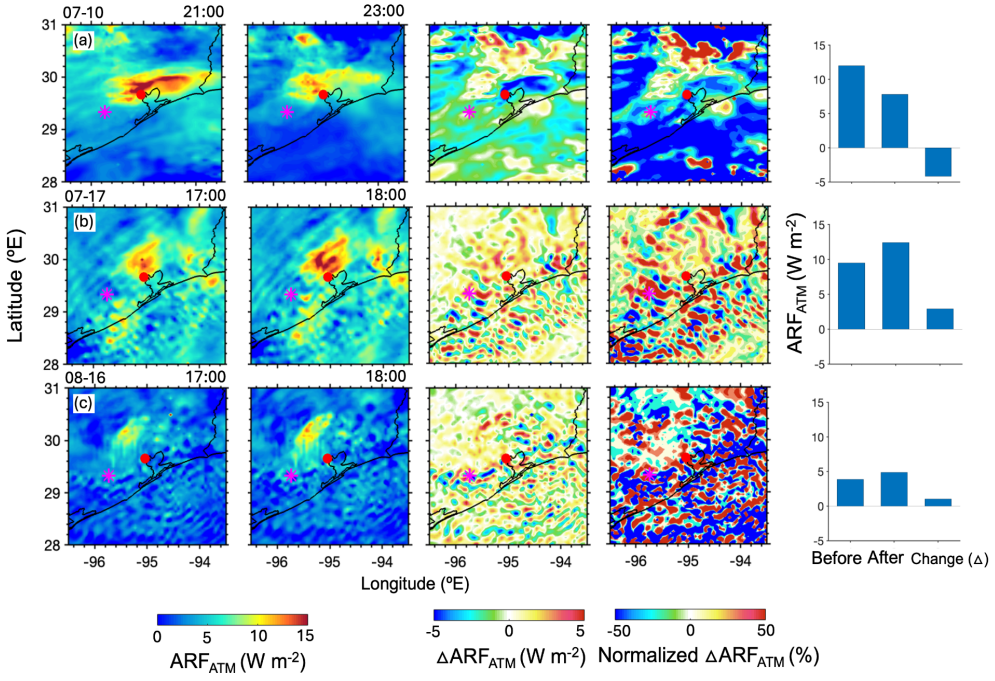

Figure 12. Spatial distribution of aerosol radiative forcing in the atmosphere (ARF_{ATM}) before (1st column), after (2nd column) SBF's passage, corresponding change (after-before) (3rd column), and the normalized change (4th column) on (a) 10 July, (b) 17 July, and (c) 16 August. The 5th column shows ARF_{ATM} at the M1 site.

https://doi.org/10.5194/egusphere-2025-2659
Preprint. Discussion started: 27 June 2025

Table 1. Model configuration

Simulation period	1 July - 30 August 2022
Domain	26 to 33 ºN and -98 to -92 ºE
Horizontal resolution (dx)	5 x 5 km
Vertical resolution	45 layers from 1000-50 mb
Meteorological initial and boundary conditions	North America mesoscale (NAM) forecast output at T221 (32-km) resolution, 28 vertical levels (Bauman, 2010)
Shortwave radiation	Goddard shortwave radiation scheme (Chou et al., 1998)
Longwave radiation	The rapid radiative transfer mode (RRTM) (Mlawer et al., 1997)
Land surface	Community National Center for Environmental Prediction (NCEP), Oregon State University, Air Force, and Hydrologic Research Lab-NWS Land Surface Model (NOAH) (Chen and Dudhia, 2001)
Surface Layer	Monin-Obukhov (Monin and Obukhov, 1954; Janjic, 2002)
PBL	Yonsei University Scheme (YSU) (Hong et al., 2006)
Cumulus	The Grell scheme (Grell and Devenyi 2002)
Microphysics	Morrison 2-moment scheme (Morrison, 2005)
Chemical mechanism	RACM Chemistry with MADE/VBS aerosols using KPP library along with the volatility basis set (VBS) used for Secondary Organic Aerosols (Stockwell et al., 1990; Ackerman et al., 1998; Schell et al., 2001)
Chemical initial and boundary conditions	MOZBC from the Model for Ozone and Related chemical Tracers (MOZART) model (Emmons et al., 2010)
Anthropogenic emissions	National Emissions Inventory (NEI), U.S. Environmental Protection Agency (EPA)
Biogenic emissions	The Model of Emissions of Gases and Aerosols from Nature version MEGAN v2.1 biogenic emissions (Guenther et al., 2012)